GRI-03/0065 vol. 2

Seal Control of Hydrocarbon Migration and its Physical and Chemical Consequences

VOLUME II: GEOLOGY, GEOPHYSICS, GEOCHEMISTRY, AND GOCAD DATABASE

FINAL TECHNICAL REPORT
(6/19/1997-12/31/2001)

Prepared by:
L. M. Cathles, M. Wizevich, and S. Losh

Cornell University
Department of Earth & Atmospheric Sciences
Snee Hall
Ithaca, NY 14853

OSP #32006

Prepared for:

GAS RESEARCH INSTITUTE
5097-260-3787

December 2002

REPORT DOCUMENTATION PAGE

Form Approved
OMB No. 0704-0188

1. REPORT DATE *(DD-MM-YYYY)*
12/16/2002

2. REPORT DATE
Final Technical Report

3. DATES COVERED *(From - To)*
06/19/1997-12/31/2001

4. TITLE AND SUBTITLE
Seal Control of Hydrocarbon Migration and Its Physical and Chemical Consequences

Volume II: Geology, Geophysics, Geochemistry and GoCAD Database

5a. CONTRACT NUMBER

5b. GRANT NUMBER
5097-260-3787

5c. PROGRAM ELEMENT NUMBER

6. AUTHOR(S)
Cathles, Lawrence, M., III
Wizevich, Michael C.
Losh, Steven

5d. PROJECT NUMBER

5e. TASK NUMBER

5f. WORK UNIT NUMBER

7. PERFORMING ORGANIZATION NAME(S) AND ADDRESS(ES)
Cornell University
Office of Sponsored Programs
115 Day Hall
Ithaca, NY 14853

8. PERFORMING ORGANIZATION REPORT NUMBER
OSP #32006

9. SPONSORING/MONITORING AGENCY NAME(S) AND ADDRESS(ES)
Gas Research Institute
1700 South Mount Prospect Road
Des Plaines, IL 60018-1804

10. SPONSOR/MONITOR'S ACRONYM(S)
GTI, GRI

11. SPONSORING/MONITORING AGENCY REPORT NUMBER
GRI-03/0065 vol. 2

12. DISTRIBUTION AVAILABILITY STATEMENT

13. SUPPLEMENTARY NOTES

14. ABSTRACT
The geology of the "GRI corridor", a 125 x 200 km area in the offshore Louisiana Gulf of Mexico, is reviewed in the context of the geologic evolution of the northern Gulf of Mexico. Source rocks in GRI Corridor, are identified from the literature and their generative potential estimated. Geologic, geophysical and geochemical data newly created by us or taken from industry and government sources are compiled in a GoCAD database. New data in the GoCAD project include definition of the top of overpressure from mudweight data in 2131 wells, chemical analyses of 217 oil samples, biomarker indices and gas washing parameters extracted from this chemical data, and gas isotopic data from several of the detailed study sites in the Corridor. The top of overpressure (TOOP) is shown to be a highly surface irregular, spiky, surface. Discovered hydrocarbon reservoirs are associated with TOOP spikes. The spikes in turn are associated with salt domes. Temperature gradients which are uniform to at least 4 km depth change from ~19° to 25°C/km over distances of ~50 km in a checkerboard pattern. This change in gradient is large enough to significantly affect hydrocarbon maturation.

15. SUBJECT TERMS

16. SECURITY CLASSIFICATION OF: a. REPORT	b. ABSTRACT	c. THIS PAGE	17. LIMITATION OF ABSTRACT	18. NUMBER OF PAGES
U	U	U	SAR	52

19a. NAME OF RESPONSIBLE PERSON
Prof. Lawrence M. Cathles III

19b. TELEPONE NUMBER (*Include area code*)
607-255-7135

GRI Disclaimer

Table of Contents

Report Documentation Page (SF 298) **2**

GRI Disclaimer **3**

Table of Contents **4**

Research Summary **5**

Technical Section **7**

A. Summary 7
B. Introduction 7
C. Corridor Geology, Geochemistry, and Geophysics 8
  1. Geology of the GRI Corridor 8
  2. GoCAD Representation of the GRI Corridor Geology 14
  3. Geophysical Data 18
    a. Seafloor Temperatures 18
    b. Subsurface Temperatures 19
    c. Heat Flow 23
    d. Subsurface Pressures 24
  4. Chemical Data 29
    a. Hydrocarbon Source Beds in Northern GoM 29
    b. Proven Hydrocarbon Resources in the GRI Corridor 33
    c. The Gas-Oil Ratio (GOR) 34
D. Results and Discussion 36
E. Recommendations 38

Acknowledgements **38**

Appendix I: Data in the GRI Corridor GoCAD Project **39**

Appendix II: Loading and Use of the GRI GoCAD Project **46**

Appendix III: References for Hydrocarbon Sources in the Northern Gulf of Mexico **50**

Bibliography **51**

Research Summary

TITLE: Seal Control of Hydrocarbon Migration and its Physical and Chemical Consequences: Volume II: Geology, Geophysics, and Geochemistry, and GoCAD Database

CONTRACTOR: Cornell University

PRINCIPAL INVESTIGATOR: Lawrence M. Cathles III

REPORT PERIOD: January 1, 1997 to December 31, 2001

OBJECTIVES: The objectives of this report are:

(1) to provide a context for other reports in this series by describing the geology, geophysics and hydrocarbon distribution in the GRI Corridor (a 125 × 200 km area of the offshore Louisiana Gulf of Mexico Basin),
(2) to describe the construction and illustrate the use of a GoCAD database containing almost all the geological, physical, and chemical data collected in the umbrella GRI project, and
(3) to document and discuss spatial relationships in the GoCAD data that are important to the pattern of hydrocarbon maturation and to the nature of compartment seals.

TECHNICAL PERSPECTIVE: The interior of the northern offshore Gulf of Mexico Basin is divided into a complex system of variously over-pressured compartments. It is an area of active hydrocarbon generation and one of the world's most active areas of hydrocarbon exploration. Even so, there is an insufficient understanding of how hydrocarbons migrate through these pressure compartments, the nature of the impermeable seals that separate the compartments, and how the flow of gas and brine affect hydrocarbon chemistry and inorganically alter sediments. In fact, the scientific community lacks even a concise summary of the relationships between such basic basin features as salt distribution, sediment thickness, the topography of the top of overpressure, subsurface temperature, heat flow, and hydrocarbon reservoir distribution. These relationships are important as a basis for many kinds of investigations because they can provide constraints on important basin processes.

RESULTS: Temperature gradients in the GRI Corridor are on average ~22.5°C/km, but these gradients can change from ~19° to ~25°C/km over lateral distances of ~50 km. Locally the temperature gradients are remarkably coherent and extend to ~5 km depth where temperatures vary from 120-150°C.

The top of overpressure (TOOP) surface crosscuts both chronostratigraphic and inferred lithostratigraphic boundaries. Consequently the seal that forms the top of overpressure cannot be a lithologic seal, as some have proposed. Hydrocarbon reservoirs cluster near topographic highs in the top of overpressure surface. These highs cannot be predicted from hydrocarbon chemistry. At topographic highs the TOOP does not appear to be a phase boundary. The spiky highs in the TOOP do seem to be leak points, which are temporally persistent once established.

TECHNICAL APPROACH: Stratigraphic, fault, temperature, heat flow, and overpressure data were compiled at the same spatial scale in a GoCAD database. The stratigraphic data were taken from a variety of sources: theses, 2D seismic interpretations, 3D seismic surveys, well log data, and donated company maps. Top of overpressure was determined by computing the depth of the effective stress equivalent of the 12 ppg mudweight at zero water depth (a proxy for the top of overpressure) in 2131 Corridor wells, based on purchased header logs. An equivalent 12 pound per gallon mudweight surface was constructed by krigging these datapoints in GoCAD. We wrote C+ macros to extract temperature and hydrocarbon reservoir data from the MMS ArcView Database and add it to the GoCAD database.

PROJECT IMPLICATIONS: Local temperature gradient variations from 19° to 25°C/km are large enough and extend deep enough to strongly affect hydrocarbon maturation. Understanding the cause of these variations sufficiently to predict them over time is clearly necessary if accurate models of hydrocarbons generation are to be constructed.

Hydrocarbon reservoirs are preferentially located near topographic highs in the top of overpressure surface. The top of overpressure can be mapped seismically. Focusing exploration near topographic highs in the TOOP should increase exploration effectiveness.

PROJECT MANAGERS: Richard Parker and Robert Siegfried

Technical Section

A. Summary

The geology of the study area for this project, which we term the "GRI Corridor," is reviewed in the context of the geologic evolution of the northern Gulf of Mexico. Source rocks in the 125 x 200 km GRI Corridor, are identified from the literature. Their generative potential is estimated at 1400 billion barrels of oil and 8600 TCF of gas. Geologic, geophysical and geochemical data newly created by us or taken from industry and government sources are compiled in a GoCAD database. The construction of this file is available as part of this GRI project. Some of the implications of the spatial relations in the GoCAD file are discussed in this report; others are the basis of much more extensive discussion in other reports in this series. New data in the GoCAD project include definition of the top of overpressure from mudweight data in 2131 wells, chemical analyses of 116 oil samples, biomarker indices and gas washing parameters extracted from the chemical data, and gas isotopic data from several of the detailed study sites in the Corridor. Conclusions reached in this report include: (1) The spikes in the top of overpressure surface are not defined by hydrocarbon phase separation but the intervening low areas may be; (2) Hydrocarbon fluids appear to be drawn toward topographic highs (spikes) in the top of overpressure which act as persistent leak points; (3) Temperature gradients can change from ~19° to 25°C/km over distances of ~50 km in a checkerboard pattern, which would dramatically affect hydrocarbon maturation.

B. Introduction

This report summarizes the geology and geophysics of the GRI Corridor, describes the GoCAD database into which we have assembled these data, and draws project-relevant conclusions. It is one in a series of reports that describe our efforts to understand physical and chemical processes in the GRI Corridor. The title of the report series is "Seal Control of Hydrocarbon Migration and its Physical and Chemical Consequences." The six (6) volumes that comprise this report are:

- Volume I: Executive Summary
- Volume II: Geology, Geophysics, Geochemistry and GoCAD Database
- Volume III: Organic Geochemistry
- Volume IV: Gas Washing of Oil and Its Implications
- Volume V: A Modeling Analysis of the Hydrocarbon Chemistry and Gas Washing, Hydrocarbon Fluxes, and Reservoir Filling
- Volume VI: A Theoretical Analysis of the Inorganic Alteration by the Flow of Brines Through Basin Seals

Published reports from a preceding GRI project describe our concepts of capillary sealing (Cathles, 2001), laboratory investigations of capillary sealing (Shosa and Cathles, 2001), methods for interpreting the history of fluid overpressuring from porosity profiles (Revil and Cathles, 2001), geochemical models of phase fractionation (Meulbroek, 1997; Meulbroek, 1998), and implications of capillary sealing for oil production (Erendi and Cathles, 2001).

Our purposes in this report are to provide a geological context for the data interpretation and modeling carried out in the other reports in this series, to present a geographically referenced version of the geological, physical (especially top of overpressure data), and geochemical data assembled under the GRI contract, and to draw several immediate conclusions from correlations between some of the data sets that we have compiled.

C. Corridor Geology, Geochemistry, and Geophysics

1. Geology of the GRI Corridor

The Gulf of Mexico opened in two episodes of rifting. The first occurred in the late Triassic-early Jurassic, and the second in the middle Jurassic. The cumulative extension of the two rifting events exposed oceanic crust on the abyssal plain south of the Sigsbee knolls. The location of the oceanic-continental crust transition beneath the thick sedimentary section of the slope is not known. At the end of the Cretaceous, the Gulf was uplifted and intruded by alkalic magmas, perhaps as the result of the passage of a mantle plume. Alkalic igneous rocks and volcanic centers of late Cretaceous age occur near Austin, Texas, along the Balcones Fault Zone to the southwest, and in northern and offshore Lousiana.

The Triassic rifting that opened the Gulf of Mexico disrupted a basement of middle Paleozoic carbonates on the east, Pennsylvanian and older clastics and carbonates on the north, and crystalline rocks on the west (Woods, Salvador et al., 1991). Redbeds, together with shale, sandstone, conglomerate, and volcanic rocks accumulated on basement to thicknesses of >2000 meters (Salvador, 1991). Locally, lacustrine muds (e.g., the Eagle Mills in Texas) are source rocks.

The middle Jurassic rifting produced a highland, now beneath the basin center, which created a restricted basin whose axis presently lies beneath the continental slopes of Texas and Louisiana. Up to 4 km of Louann Salt accumulated in this basin, and the Werner anhydrite was deposited on its margins (Salvador, 1991; Peel, Cole et al., 2001). The salt filled an irregular topography and its thickness varied accordingly. Overall, the in-place original salt thickness ranged from near zero at the northern edge of the basin (now southern Arkansas) to 4 km along the present continental slope.

The sedimentation that followed salt deposition was initially slow and its organic content high, perhaps because brine pools inhibited oxidation. The upper Jurassic (Oxfordian, e.g, the lower Smackover Formation, Kimmeridgian, and Tithonian) carbonates and marls that were deposited at this time are the most important source rocks in the GRI Corridor. Growth faults that affect formation thickness indicate that salt movement began with this sedimentation, but salt stocks did not form until late Cretaceous time with the onset of rapid sediment deposition from the uplifted Rocky Mountians (McBride, 1998).

Carbonate deposition dominates the Cretaceous. Reefs built to 4 km thickness around the basin periphery. Carbonate thickness on the shelf was variable, due largely to salt movement, but was generally less than 2 km (McFarlan and Menes, 1991). At the end of the Cretaceous a major sea level regression exposed the shelf to widespread erosion. This produced a strong seismic reflector that forms a marker throughout the northern Gulf of Mexico known as the “MCSB” or “mid-Cretaceous sequence boundary.” Some workers interpret the “MCSB” as a late Cretaceous feature (Colling, Alexander et al., 2001).

Toward the end of the Cretaceous, the Laramide orogeny began to drive clastic deposition in the western and northwestern Gulf. This soon overwhelmed carbonate deposition and consequently Cenozoic deposition is entirely siliciclastic (Winker, 1984; Salvador, 1991; Feng, Buffler et al., 1994). Sediments were deposited mainly in a series of deltas which shifted position from west to east as the Mississippi River drainage became progressively better organized (Diegel, Karlo et al., 1995). Positions of the shelf edge and major Cenozoic depocenters are shown in Figure 1. The GRI Corridor is located in an area which received sediments from the Central and Eastern Mississippi deltas starting in the early Miocene.

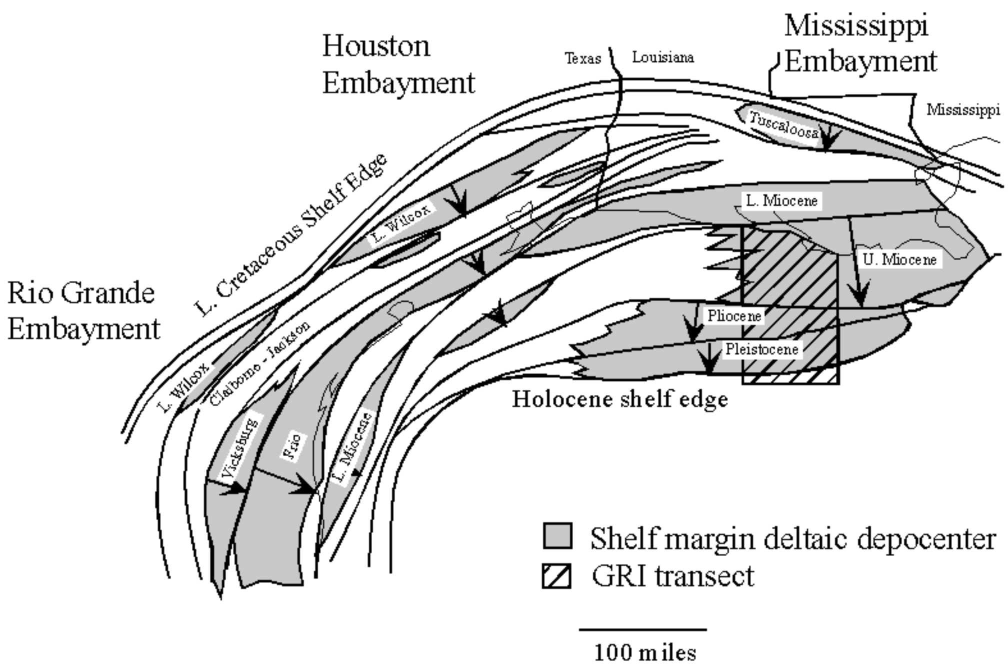

Figure 1. Positions of the shelf edge and major Cenozoic depocenters in the northern Gulf of Mexico Basin. Modified from Galloway, Bebout et al. (1991) and Winker (1982).

The rapid post-Laramide siliciclastic sediment loading drove major salt migration. The style of sedimentation and structural deformation at this stage is controlled largely by position relative to the prograding shelf edge (Galloway, Ganey-Curry et al., 2000). Sandy *delta plain deposits*, consisting of distributary channel sands, crevasse splays, levees, and interdistributary muds, extend from the shoreline to the shelf edge. *Progradational delta-fed apron deposits* lie basinward of the shelf edge. These consist of delta front sands, delta fringe sands, and, predominantly, prodelta shales. In this area, sedimentation drove salt migration, and sediment thickness is strongly affected by ~20 km diameter minibasins that form where salt withdraws into walls, stocks and overhangs. *Basin floor aprons* are deposited basinward of the slope. During glacial lowstands in the Pleistocene, channels were incised into the shelf, which transported sandy sediments across the shelf and deposited them in basin floor fans.

Structures reflect the escape of salt and the basinward sliding of sediments (Figure 2). Long listric growth faults subparallel to the shoreline are abundant on the Texas Gulf coast and portions of Louisiana. These sole into shales or into now-evacuated, but once-continuous, salt sheets. A complex arcuate fault geometry reflects minibasin formation. Compressional tectonic structures (contractional regimes in Figure 2) are found on the downdip toes of the salt sheets.

As shown in Figure 2, the GRI Corridor lies mainly within the Salt Dome/Minibasin province, with its northwestern corner lying in the Miocene detachment province and its southern third in the Plio-Pleistocene detachment province. Major basin floor canyons lie east and west, flanking the GRI Corridor, but there are none in the Corridor. Rowan and Weimer (1998) document Pleistocene channels along the outer shelf and upper continental slope of the Corridor.

The geological history is summarized by two cross sections whose positions are indicated in Figure 2. The longest of these sections runs a distance of 1050 km from the Arkansas-Louisiana border to the Sigsbee Knolls, an outcropping of allochthonous salt at the southern margin of the basin. This section, shown in Figure 3, is based on 2D seismic and well bore data, and was constructed by Exxon and given to the GBRN for use in this and other projects in 1991. It shows time-stratigraphic horizons mapped seismically and tied to well log data, and illustrates how a ~16 km thick sedimentary wedge built and extended Gulf-ward starting in early Cretaceous time. It depicts the upper portions of large-scale detachment faults in schematic fashion. The top of overpressure, compiled from mud weight and literature reports, forms an irregular surface that rises to both north and south from a maximum depth near the present shoreline of ~6000 m. The upper Jurassic and Eocene hydrocarbon source beds, discussed below, are indicated by red and orange lines respectively.

Figure 4 shows regional aspects of salt distribution in a more detailed section constructed by McBride (1998). Allochthonous salt sheets extend across the entire shelf and part of the slope, but not into deeper water areas further south. In the south the salt sills are sourced directly from the Louann Salt. The section implies that a series of salt sills formed sequentially from north to south and were evacuated in the northern and middle portions of the section. For example, as shown by McBride (1998), a restricted salt canopy formed in the northern part of the section during the Eocene and was evacuated during the Oligocene and Miocene. The Timbalier salt sheet formed basinward of this in the middle Miocene and was evacuated during the late Miocene and Pliocene. Further south a more extensive sill formed in the late Miocene and was evacuated from the late Miocene to Pleistocene. The deep-water sills that are near the surface today are only now being loaded by sediment and evacuated by lateral and vertical salt migration.

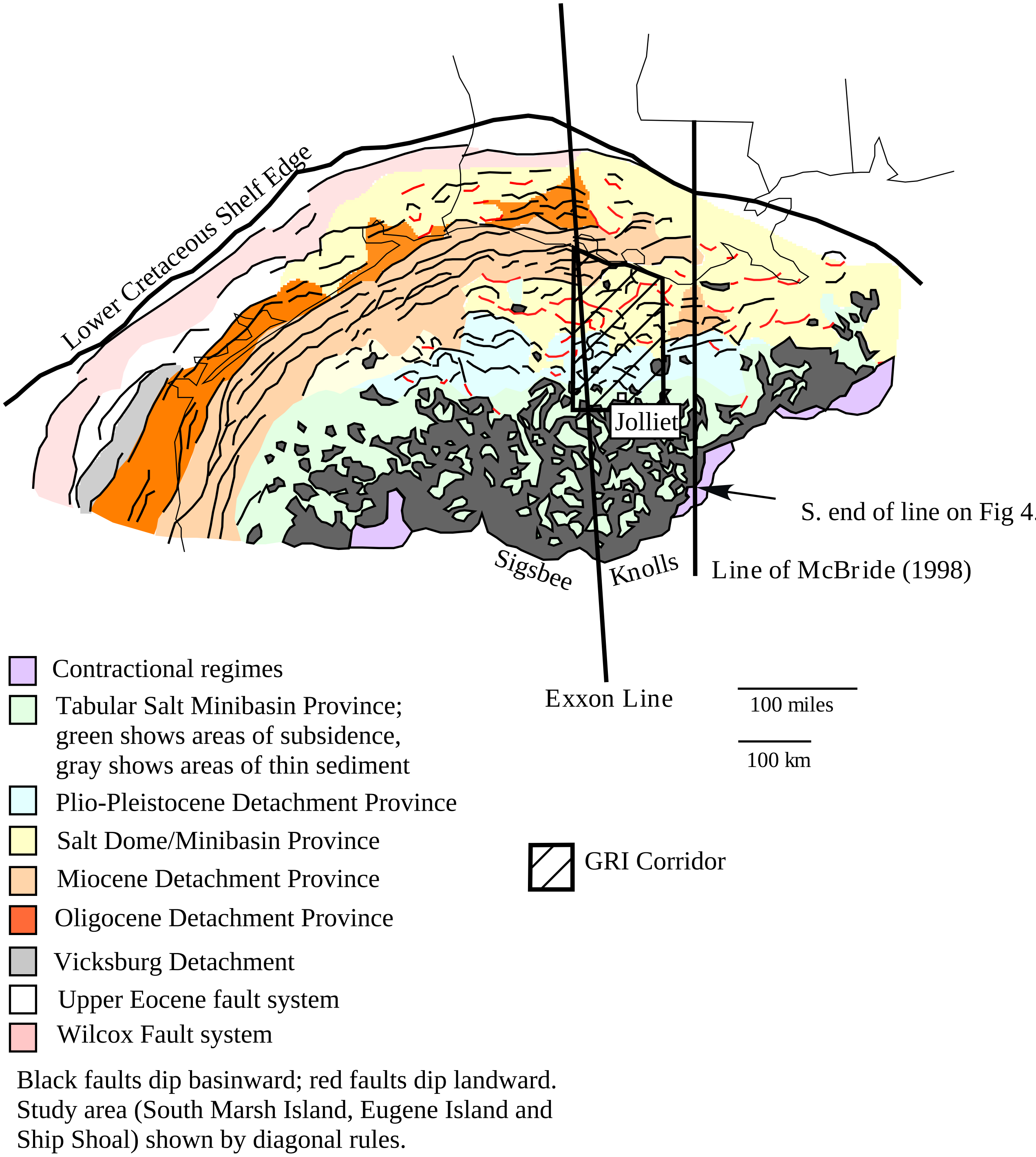

Figure 2. Tectonostratigraphic map of the norther Gulf of Mexico Basin. Modified from Diegel et al (1995). GRI Corridor is shown by hatches. Sections are shown in Figures 3 and 4.

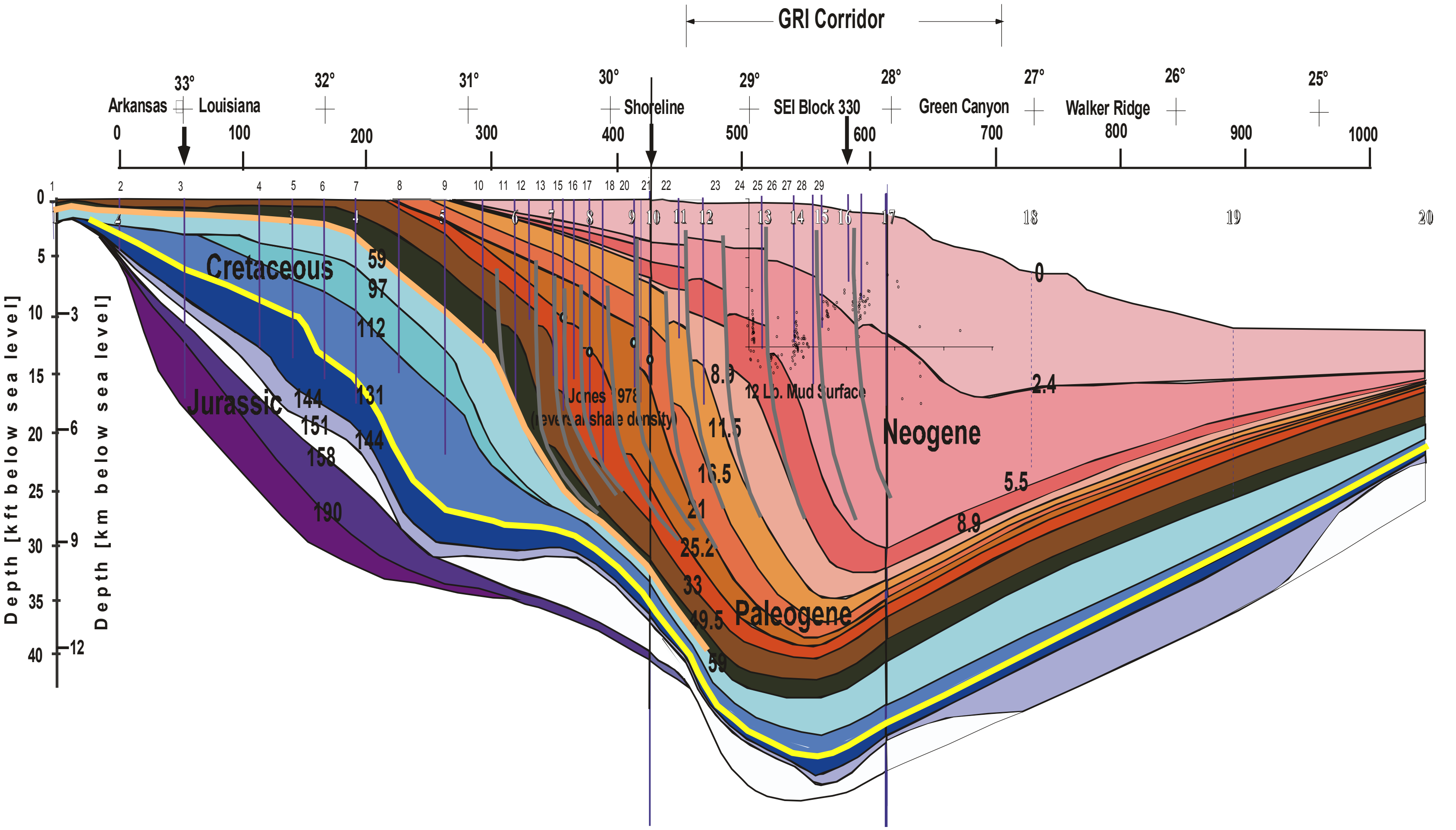

Figure 3. Time-stratigraphic horizons in the 1050 km long Louisiana section located in Figure 1. The section is based on 2D seismic and well bore data, and was constructed by Exxon and given to the GBRN for use in this and other projects in 1991. The Upper Jurassic and Eocene source strata are indicated by yellow and orange lines respectively.

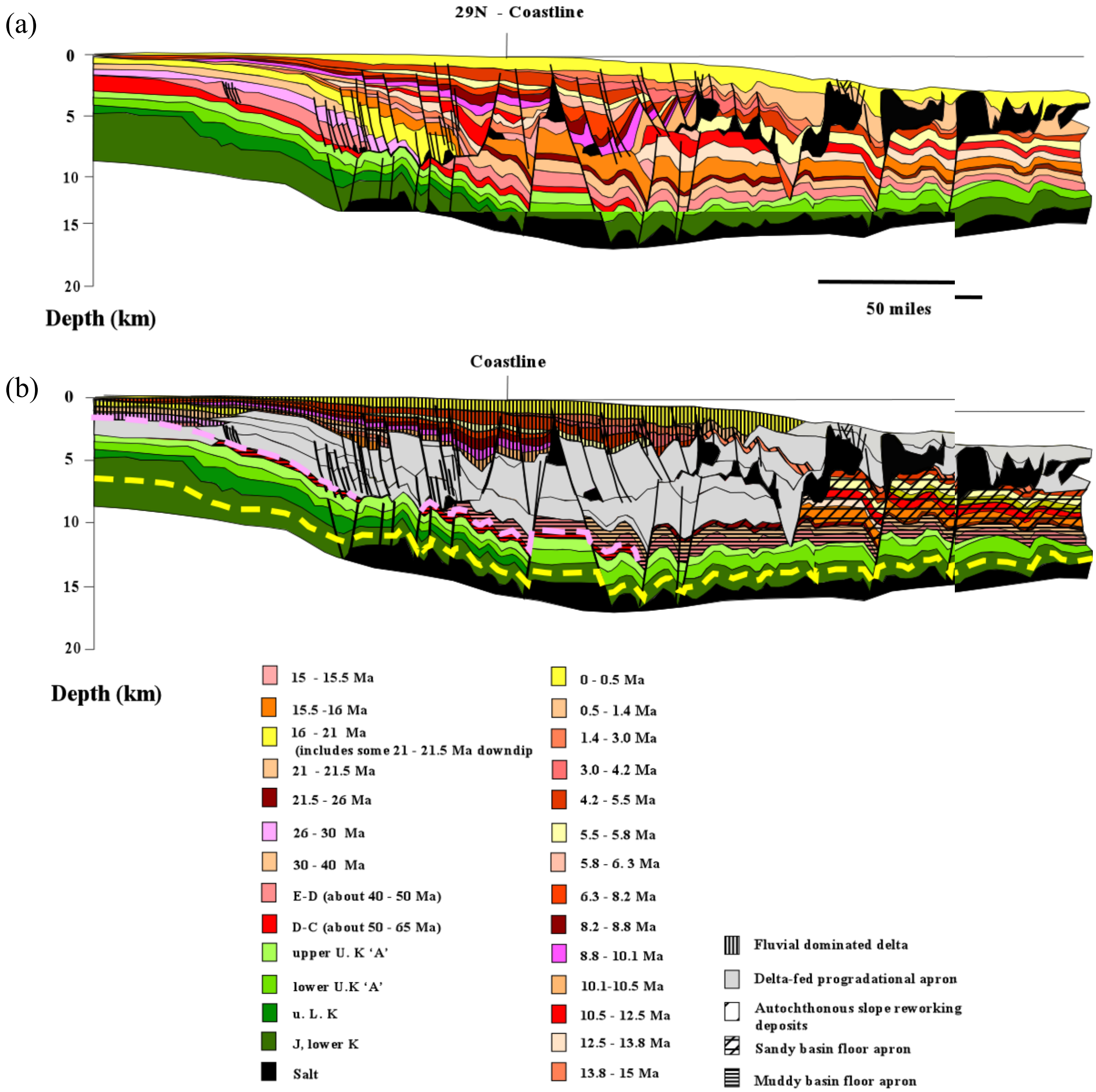

Figure 4. (a) North-south section modified from McBride (1998). Section is located in Figure 2. (b) System tracts of Galloway et al. (2000) are superimposed on the time-stratigraphic intervals in the lower section. The Upper Jurassic and Eocene source strata are represented by yellow and pink dashed lines respectively.

Others extend a single Eocene salt sheet only part way across the present shelf (Peel et al., 1995), or extend a single Eocene sill across the entire section (Diegel et al., 1995). These interpretations are not consistent with strata and/or salt thickness in our compiled Corridor data, whereas McBride's (1998) interpretation is. We believe therefore that McBride's summary is the best published general synthesis for the Corridor. Figure 4b overlays the systems tracts mapped by Galloway et al. (2000) on the McBride section and provides a basis for assigning sand:shale ratios.

2. GoCAD Representation of the GRI Corridor Geology

A major part of this project was compilation of the GRI Corridor Geology in the GoCAD software package (http://www.t-surf.com/). GoCAD allows effective investigation of 3D aspects of geologic data. Geochemical data (or any other kind of data) can be displayed against selected horizons and faults and rotated, zoomed, and otherwise manipulated. GoCAD has powerful krigging, cross-plotting, and other statistical capabilities, and illustrations can be easily generated and pasted in reports. GoCAD is an industry standard application, which should make compilations in this software particularly valuable to industry. The geologic data described below, all of the geochemical data assembled and produced in this project, and a new top of overpressure map we have generated, have been placed in a GoCAD project file called *Gri_Final.prj*. The data included in the GoCAD project file is described in Appendix 1. The loading and use of this project file is described in Appendix 2.

The compilation of Corridor geologic data into GoCAD was done at two scales: Fourteen horizons and top and bottom of salt were digitized across the entire GRI Louisiana Corridor. The stratigraphic data was derived from two seismic cross sections published by Rowan (1996), four regional seismic lines contributed by Arco, and a salt compilation by Simmons (1992), as described by Cornelius et al. (in press). Although they are of low resolution compared to industry data, the regional surfaces in the GoCAD project fit detailed 3D seismic interpretation in the Corridor quite well.

More detailed geologic interpretations were captured in GoCAD at four sites in the Corridor. Three industry 3D seismic surveys were provided at Tiger Shoals, South Eugene Island Block 330, and Jolliet. We interpreted these surveys and calibrated them against well and biostratigraphic data provided with the seismic data (Tiger Shoals) or acquired separately (Eugene Island area: Holland, Leedy et al., 1990; Alexander and Flemings, 1995; Alexander and Handschy, 1998; Jolliet: Cook and D'Onfro, 1991). In the Eugene Island Block 330 area, we extended the 3D seismic horizons by digitizing four regional scale (~50 km E-W by ~130 km N-S) index fossil maps (Trim. A, Plan. X, Ang. B, and Lentic) provided by Texaco. The geology around South Marsh Island 9 was compiled from structure contour maps provided by Chevron. In that area, we have little age control.

All the time-stratigraphic surfaces that we have digitized and imported to GoCAD are listed according to their age in Table 1. Figure 5 shows the GoCAD representation of the top of salt surface in the GRI Corridor and the stratigraphic horizons from the 4 sites where we constructed more detailed GoCAD geologic models. The Corridor geology and the detailed site geology provide a reference for interpretation of the geochemical data and a basis for modeling. These are reported separately in this report series.

Figure 6 illustrates, in perspective view, the very different geology at the 4 sites. The Tiger Shoals area is characterized by more or less flat-lying sediment that is only slightly faulted. At South Marsh Island Block 9, a salt diapir dramatically punches through the stratigraphy. South Eugene Island Block 330 is a classic salt withdrawal minibasin, with regional and counter-regional faults forming the northern and southern boundaries of the basin. Jolliet is a good example of a salt overhang and oil trapping in an area of active salt tectonism.

Table 1. Correlation chart for the time stratigraphic horizons that define the Corridor geology and that provide the basis for model construction. The sources of horizon data are discussed in the text. The depisodes are from Galloway et al. (2000).

	Age (Ma)	Regional	Tiger Shoals	S. Marsh Is.	S. Eugene Is.	**TEXACO**	Jolliet	**Depisode**
Pleistocene	0	Horizon 14						
								0.1
	0.4						CZ	Sangamon
	0.46	Horizon 13			P. Lac. A			
								0.6
	0.65				P. Lac. B	Trim. A		
	0.75	Horizon 12				(0.4-1.1 Ma)	GS	
	0.9				Sm. Gep. 1			
	1							Trim. A.
	1.1						JB	
	1.2				Sm. Gep. 2[6]			
	1.27	Horizon 11			H. Sellii			
	1.4					Plan. X		
	1.5				C. Mac.	(1.1-1.7 Ma)	KS	
								1.6
	1.7	Horizon 10						
						Ang. B.		2.0
L. Pliocene						(1.7-2.2 Ma)		*Angulogerina* B
	2.2				Lentic 1			
								2.3
						Lentic		
						(2.2-2.8 Ma)		*Lenticulina*
	2.8	Horizon 9						
								3.1
	3.4							*Globoquadrina*
E. Pliocene	3.7	Horizon 8						*altispira*
	4	Horizon 7						
								4.2
U. Miocene	5.4	Horizon 6	Tex X	?10200' sand				*Buliminella* 1
	6			?cp-9 sand				
				?12200' sand				
								6.4
	7			?15600' sand				
				?16100' sand				
	7.4		Big A	?17300' sand				L. Miocene
	8							
	8.3	Horizon 5						
	9							
	9.6		Tex L.					
	10							
M. Mio.	13.4	Horizon 4						12
	14.6		C. opima					M. Miocene
								15.6

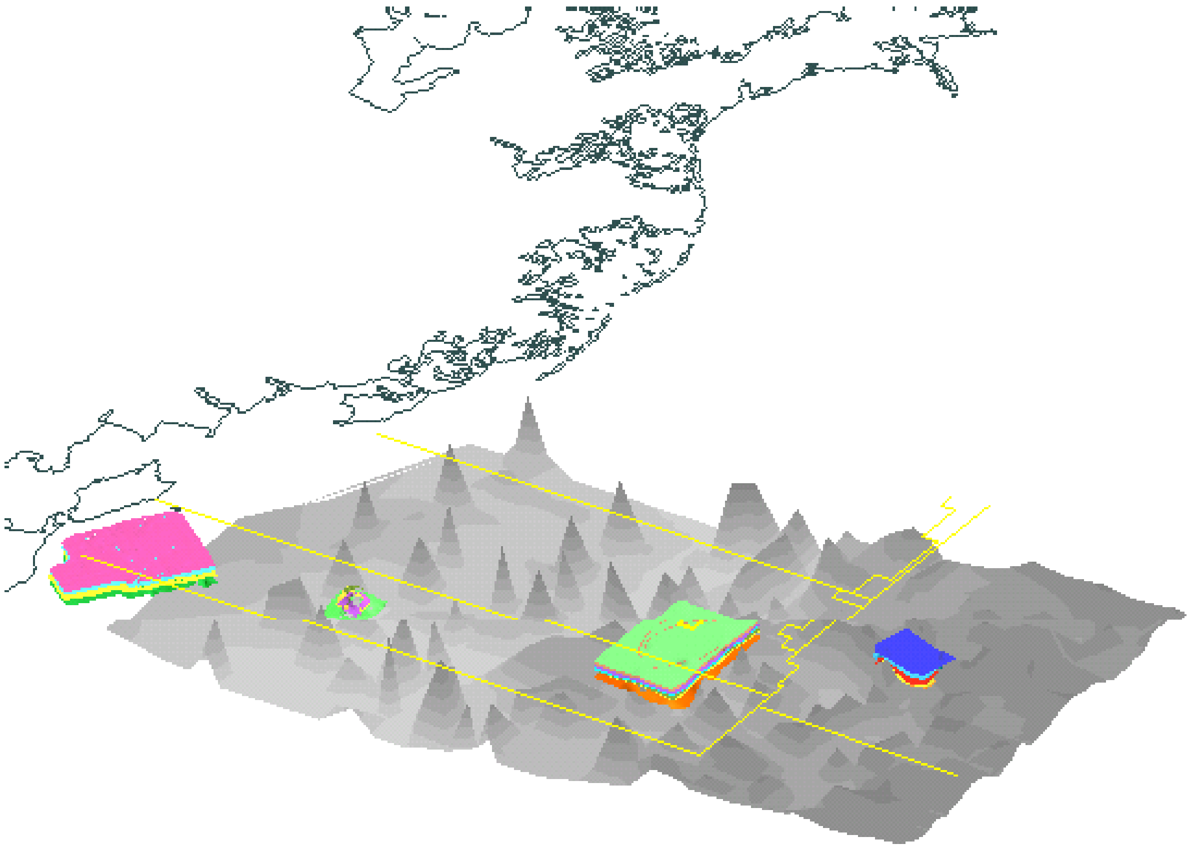

Figure 5. Top of salt in GRI Corridor, with overlying strata from the Tiger Shoals, SMI 9, SEI 330 and Jolliet detailed study areas. Perspective view looks northeast.

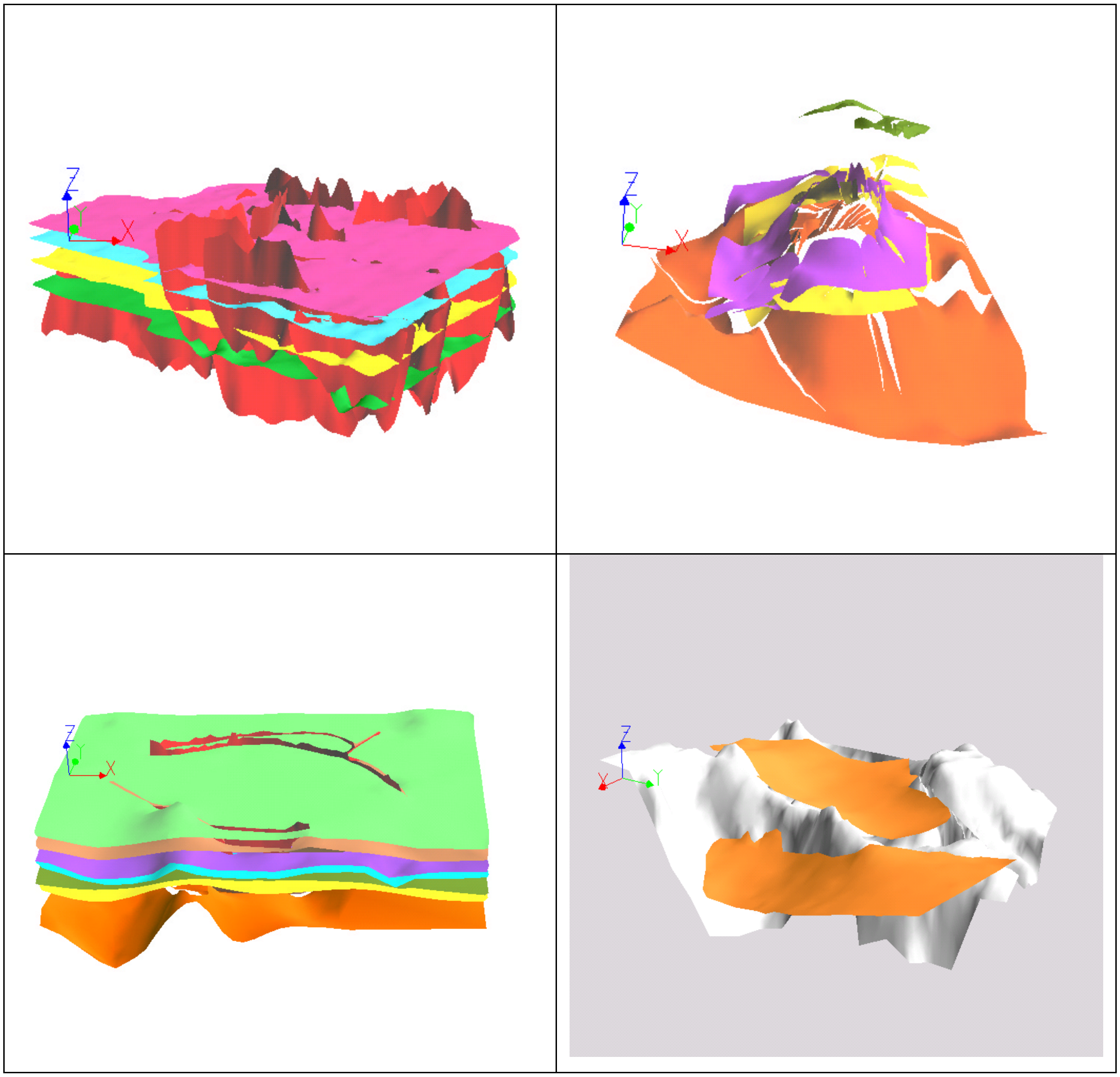

Figure 6. Perspective views of the detailed geology we have compiled at Tiger Shoals (upper left), South Marsh Island 9 (upper right), the South Eugene Island Block 330 area (lower left), and Jolliet (lower right). All are at 3x vertical exaggeration. The orange horizon at Jolliet is the KS horizon, and salt is white in that figure.

3. Geophysical Data

Basic physical data on seafloor and subsurface temperature, surface heat flow, and subsurface pressure are critical to understanding hydrocarbon maturation and the nature of basin seals. This section compiles these data.

a. Seafloor Temperatures

Subsurface temperatures increase with depth starting from the average temperature of the sea floor. The seafloor temperature varies from ~25 to 5°C in the offshore Louisiana Gulf of Mexico. Semi-yearly variations in bottom water temperature of up to 10°C occur on the shelf, but averaged over several years, the seafloor temperature is a function of water depth only. This is demonstrated by temperature-depth profiles from a few to ~100 meters below the surface that were collected by the NOAA National Marine Fisheries Service in the offshore Louisiana Gulf of Mexico between 1963 and 1965 (Temple, Harrington et al., 1977). We use these data, together with a single data point of 7°C and 540 m depth at Jolliet (MacDonald, Guinasso et al., 1994; Sassen and MacDonald, 1994) to define the relation between bottom water temperature and depth.

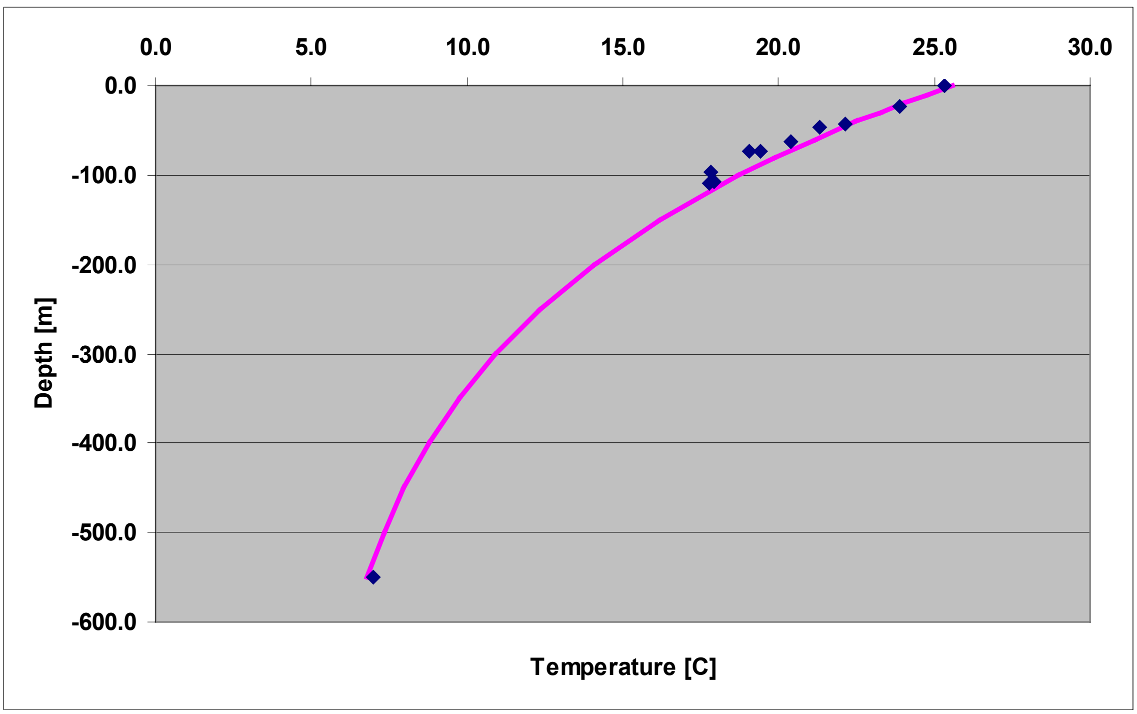

Figure 7. Average water temperatures as a function of water depth on the Louisiana Gulf of Mexico shelf. Data from Temple, Harrington et al. (1977), MacDonald, Guinasso et al. (1994), and Sassen and MacDonald (1994). The curve is specified by $T(z) = 4.3 + 21.3 \exp(0.0039z)$, where T is the water temperature and z is the elevation below sea level in meters (z is negative).

b. Subsurface Temperatures

We have assembled a temperature data set in the GRI Corridor that consists of about 500 temperature measurements from drill logs corrected by Horner method or by estimates of the proper correction (mainly in the SEI 330 area) and 2762 temperatures for specific reservoirs compiled by the MMS (Bascle, Nixon et al., 2001). These data are plotted in Figure 9 for selected parts of the Corridor to determine the average thermal gradient. The computed subsurface temperature gradient is considered if it projects to the seafloor at the bottom water temperature expected from Figure 7. Figures 8 and 9 show that the temperature gradient is ~22.5°C/km throughout the Corridor, and that, with one minor exception, the subsurface temperature trends project to the present average bottom water temperature indicated in Figure 7.

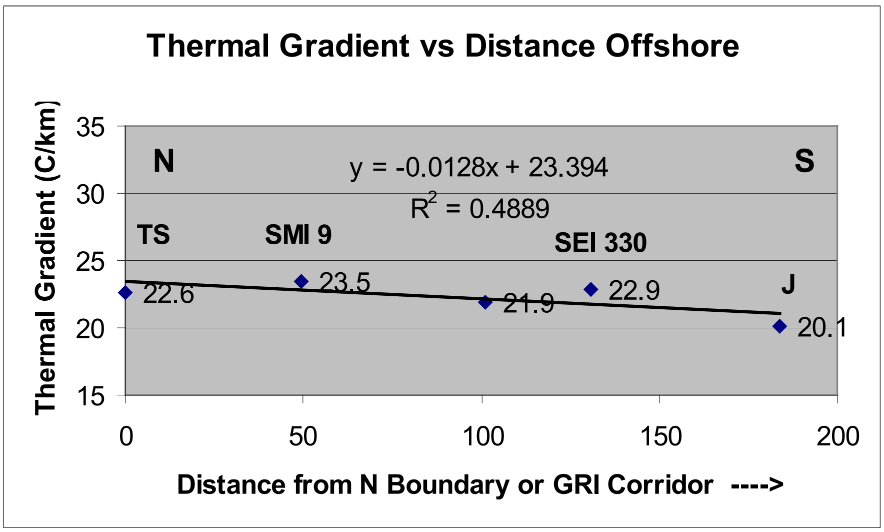

Figure 8. Subsurface temperature gradients determined at Tiger Shoals (TS), SMI 9, SEI 330, and Jolliet (J). The average temperature gradient in the GRI Corridor decreases from ~23°C/km in the north to ~20°C/km in the south.

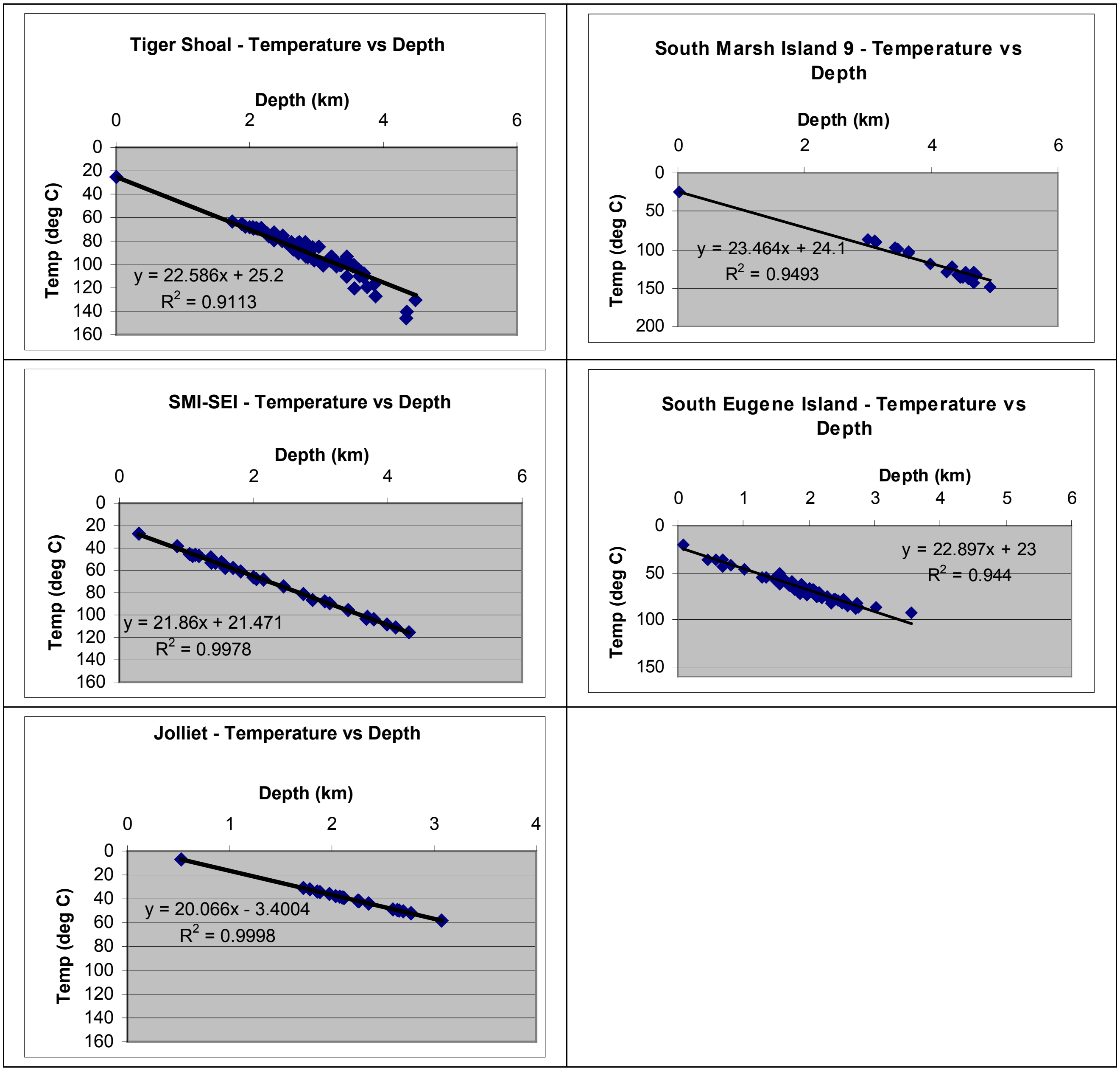

Figure 9. Temperature versus depth at the four sites summarized in Figure 8. Note subsurface temperature-depth trends generally project to the bottom water temperatures defined by Figure 7 (the shallowest data point). Data are mainly reservoir temperatures from Bascle, Nixon et al.(2001) and are the same data depicted in Figure 10.

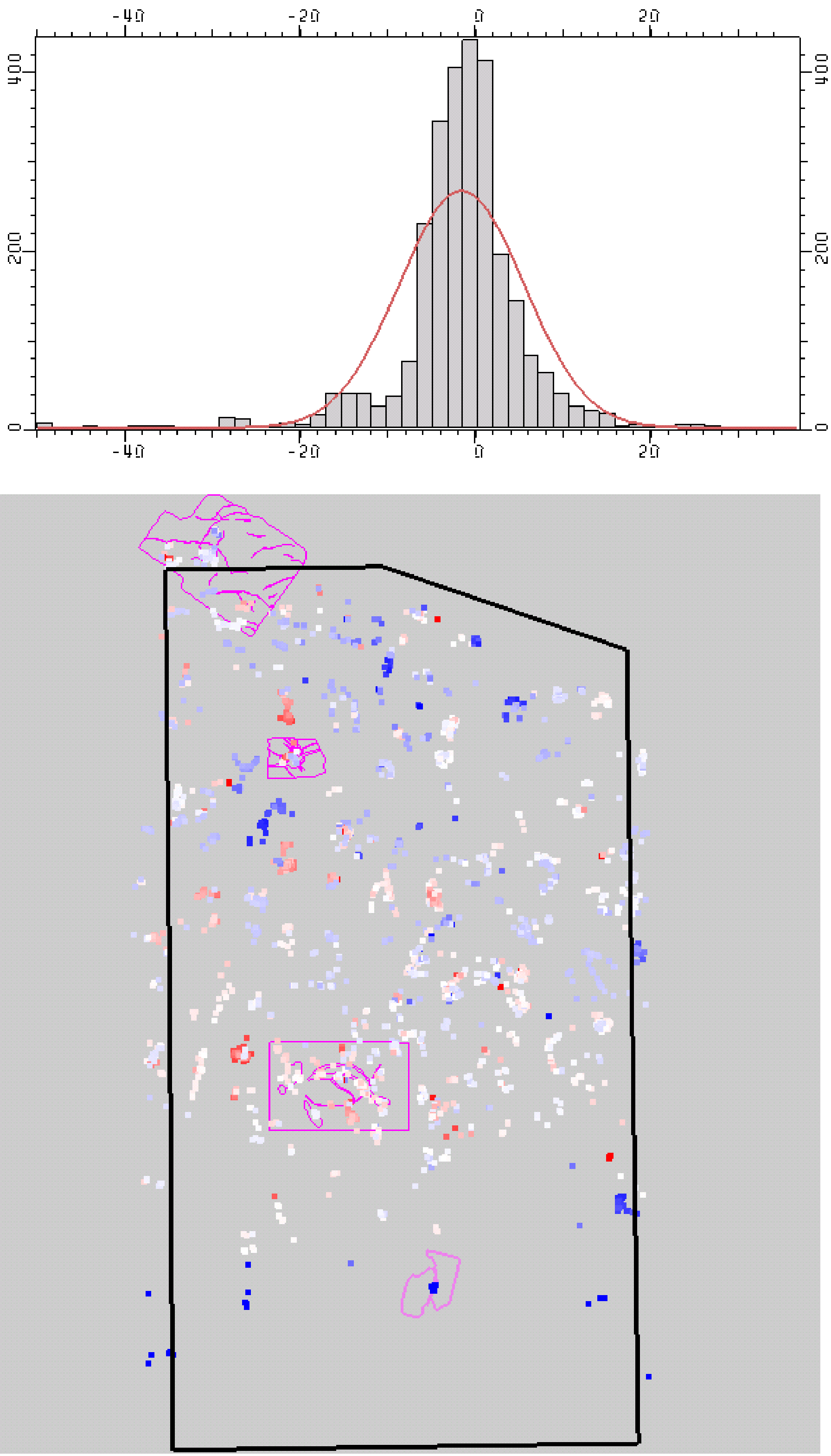

Figure 10a. Histograms of MMS (Bascle, Nixon et al., 2001) reservoir temperature deviations from those expected based on seafloor temperature (from equation 1) and 22.5°C/km temperature gradient. Deviation data are plotted in 10b, but temperature deviations are truncated at ±20°C. Red represents positive deviations (hotter than expected at the reservoir depth) and blue negative (cooler than expected at the reservoir depth). Figure 11 plots temperature against depth for data from 4 of the most anomalous sites in the immediate vicinity of SMI 9. In this area the temperature anomalies form a checkerboard pattern with ~50 km scale.

Figure 10a shows how temperatures deviate from those expected based on a constant geothermal gradient of 22.5°C/km. Temperature anomalies can be >20°C. Temperature profiles in four of the most anomalous areas clustered around SMI9 are shown in Figure 10b are plotted in Figure 11. The temperature profiles in these anomalous areas are regular and show that the cause of the deviation from average is a local variation in the temperature gradient. The temperature gradient across the Corridor is on average 22.5°C/km, but locally it can be as low as 18°C/km or as high as 25°C/km. The anomalies coincide in a general way with salt domes, but the resolution with which salt domes are defined in our database is not sufficient to determine how the domes are affecting the heat flow. The high gradient areas lie over domes, but so does one of the low gradient areas (Figure 12). None of the areas with anomalous temperature gradients lies within the coverage of one of our 3D seismic surveys.

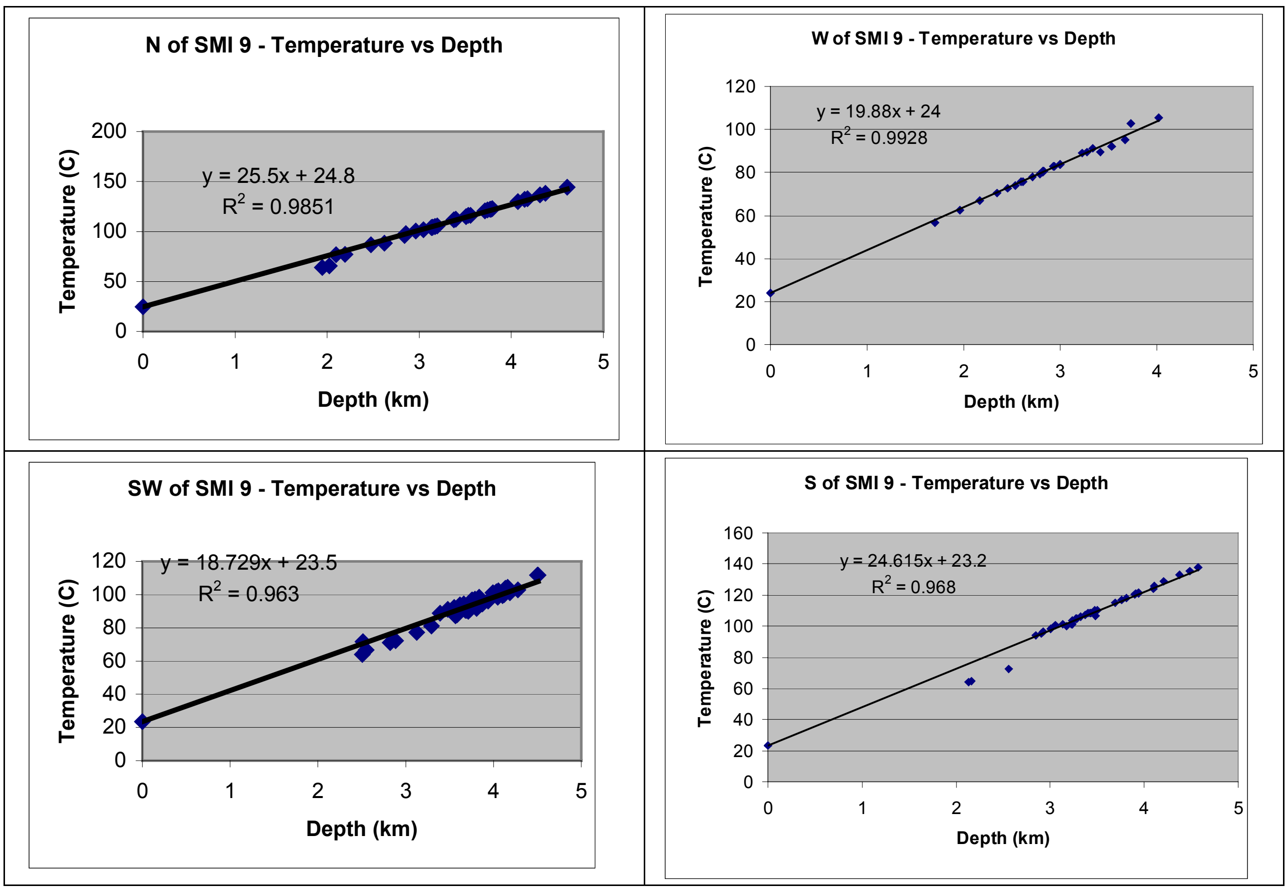

Figure 11. Temperature versus depth for data from four anomalous sites in Figure 12. Variation of the temperature gradient from 18.7 to 25.5°C/km causes the temperature departures from the average trend. Sites are located on Figure 12.

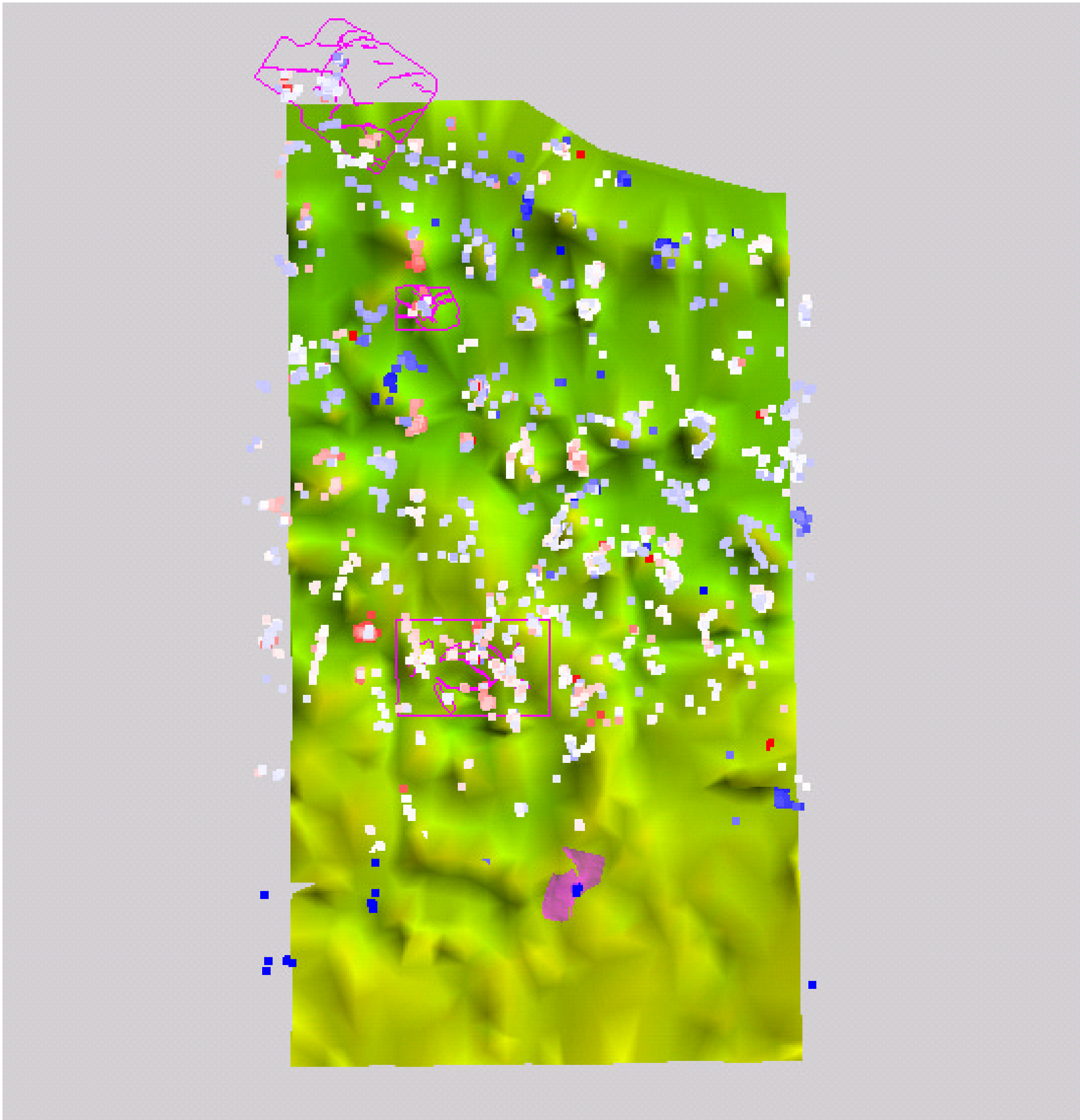

Figure 12. The temperature deviations in Figure 10b superimposed on the top of salt. The 4 anomalies (2 red positive and two blue negative) associated with SMI 9 and discussed in text are not simply explained by their position relative to salt. However, our definition of the top of salt surface is of low resolution.

c. Heat Flow

Figure 13 shows a generalized north-south heat flow profile along the Louisiana section of Figure 3. The heat flow data is compiled from several sources (Smith and Dees, 1982; Blackwell and Steele, 1992; Nagihara, Sclater et al., 1996; Colling, Alexander et al., 2001). Avoiding the obvious heat flow highs associated with salt diapirs, heat flow is about 60 mW/m^2 in northern Louisiana, drops to about 25 mW/m^2 on the shelf, and then climbs to about 43 mW/m^2 south of the Sigsbee Knolls. The very low heat flow in the center of the Figure 4 section is caused by very high recent sedimentation rates (see Report V).

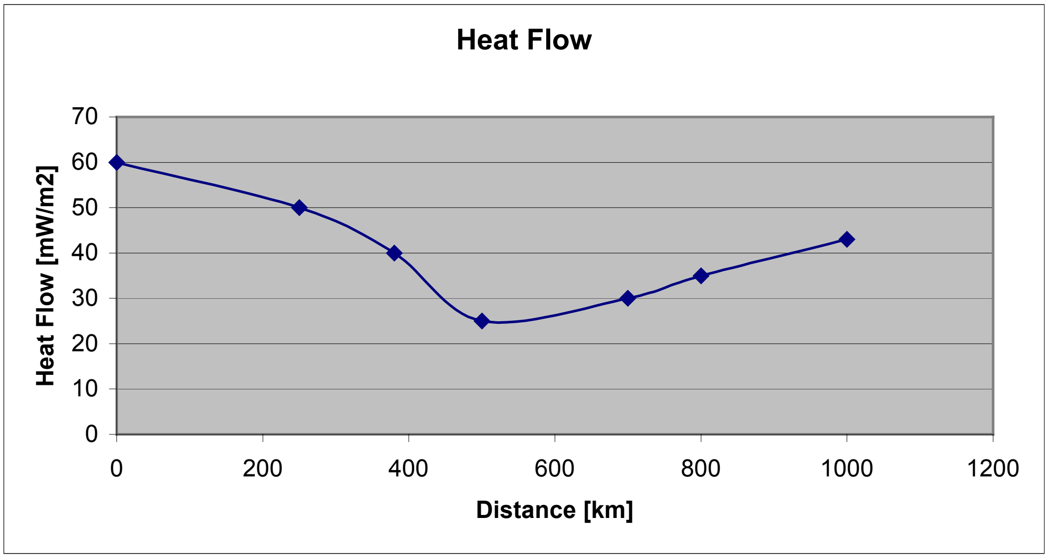

Figure 13. Heat flow data from the sources cited in the text are shown along the Louisiana Line of Figure 4.

d. Subsurface Pressures

The deeper portions of the Gulf of Mexico Basin are highly overpressured. A principal objective of this project was to understand the causes of this overpressuring, how seals divide the interior of a basin into compartments of varying levels of excess pressure, and how they maintain these differential pressures over protracted periods of geologic time.

Consequently we mapped the top of overpressure surface in the GRI Corridor by purchasing, from the Petroleum Institute (now HIS energy), header logs for 5028 wells which contained at least two mud weight measurements. Following industry practice, we use the 12 pound per gallon (ppg) mudweight as a proxy for the top of overpressure. A software program was written to interpolate mudweights in each of the 2131 wells in our dataset which had at least one mudweight >12 pounds per gallon, and so compute the expected depth at which 12 ppg mudweight was required to maintain the well. In deviated wells, we determined the true vertical depth of the 12 ppg mudweight. Where water depths were significant (>10% of the depth to 12 pound mud surface), a correction for the weight of mud in the water column pipe string was made. How we handled these two issues is the subject of the next two paragraphs.

The trajectory of a deviated well was determined from survey data where available. If survey data was not available, the trajectory was determined from the collar and bottom hole locations, measured depth, and true vertical depth by solving for the whipstock depth (the depth at which the well trajectory changed from vertical to angled) and interpolating from there to the bottom hole location. If the true vertical depth was not recorded in the header logs, the whipstock depth was estimated from the measured depth and bottom hole offset assuming a deviation of 30° from the vertical. In the absence of any indication that the well was deviated, we assumed the well was vertical.

Where water depth is significant, the weight of mud in the water column pipe string generates large pressures at shallow subsurface drilling depths. At such locations, even low mudweights can indicate near-lithostatic pressures. We corrected for the mud weight in the water column pipe string by converting all mudweights to the fraction of reduced lithostatic pressure they represent in the sediments. The reduced lithostatic pressure is lithostatic pressure minus hydrostatic pressure. A 12 ppg mudweight pressure corresponds to fraction of reduced lithostatic pressure of 0.37. Mathematically $(p_f-p_{hyd})/(p_{lith}-p_{hyd}) = 0.37$, where p_f is the aqueous pore fluid pressure, p_{hyd} is the hydrostatic fluid pressure at the depth below sea level, p_{lith} is the lithostatic pressure (the weight of the sediment solid matrix <u>and</u> all water, including the ocean column, above the point in question), and we assume a sediment density of 2.2 g/cc and a water density of 1 g/cc. We found the depth and location at which a reduced lithostatic fraction of 0.37 was exceeded in the 2131 wells in our data set. These locations were then imported to our GoCAD database and krigged to produce a 12 pound "equivalent" mud surface. By "equivalent" we mean that the pressure surface is an equivalent to the pore pressure fraction of lithostatic pressure of a 12 ppg surface where water depth is zero. All wells were corrected for water depth, but the corrections are important only where water depth is >10% of the depth of the 12ppg mudweight.

The relation of the krigged 12-ppg equivalent mudweight surface and the depth of 12 ppg equivalent mudweights in individual wells (data points) is shown in Figure 14. The 12 ppg equivalent mudweight data are coherent in that that adjacent pressure determinations are similar, but they define a highly irregular, "spiky" surface on a larger scale. The spikes can be kilometers high. The surface is so spiky that the krigged surface does a poor job of capturing the full height of the spikes, although it provides a good subdued impression of the irregularity of the surface.

Figure 15 shows that discovered hydrocarbon reservoirs tend to be located near the topographic highs in the 12 ppg equivalent mudweight surface. The outlines of the hydrocarbon reservoirs are from the MMS compilation (Bascle, Nixon et al., 2001). This relationship is discussed at greater length in a subsequent section of this report.

Figure 16 shows the relationship between the 12 ppg equivalent mudweight surface and the time-stratigraphic horizons in the GRI Corridor. The equivalent 12 ppg surface clearly cuts across stratigraphy and lithology locally at pressure spikes. For a detailed study at a particular site see Revil and Cathles (2001). The pressure surface also crosses the shelf-edge trajectory and, since lithology is tied to the shelf edge in a general way, the equivalent 12 ppg surface probably also cuts across lithology on a regional scale. Salt domes are associated with topographic highs (spikes) in the top of overpressure in most cases. Of the 23 domes in Figure 16, for example, the equivalent 12 ppg surface rises over 16, falls over 3, and shows no change over 4. Figure 17 shows that the tendency for the equivalent 12 ppg mudweight surface to be high near salt domes is a general relationship.

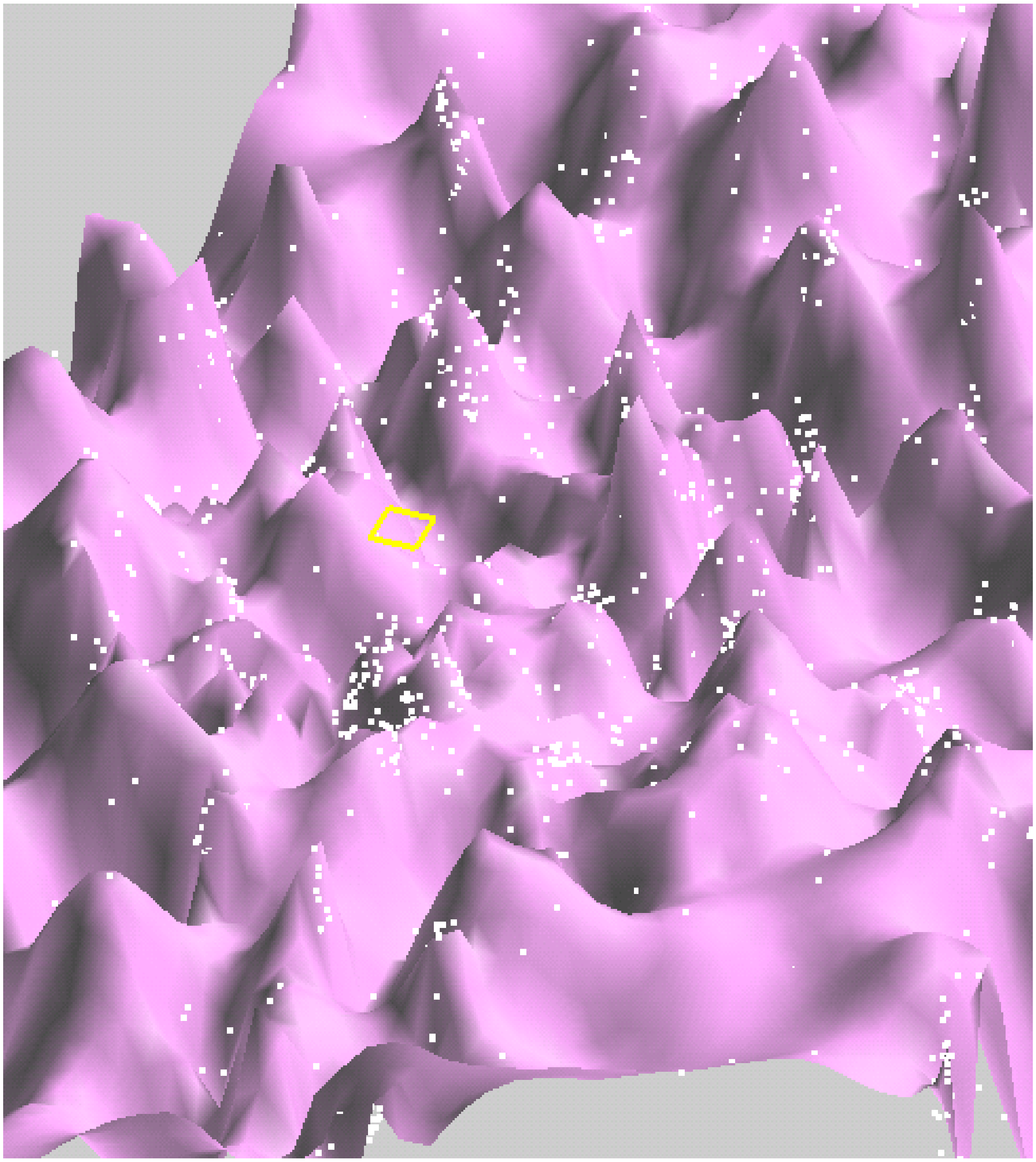

Figure 14. A subset of the data defining the 12 ppg equivalent pressure surface (white points) displayed against the krigged representation of the same 12 pound mud surface. The yellow square is South Eugene Island block 330. The krigged surface represents the pressure data reasonably well but fails to capture the full height of the peaks.

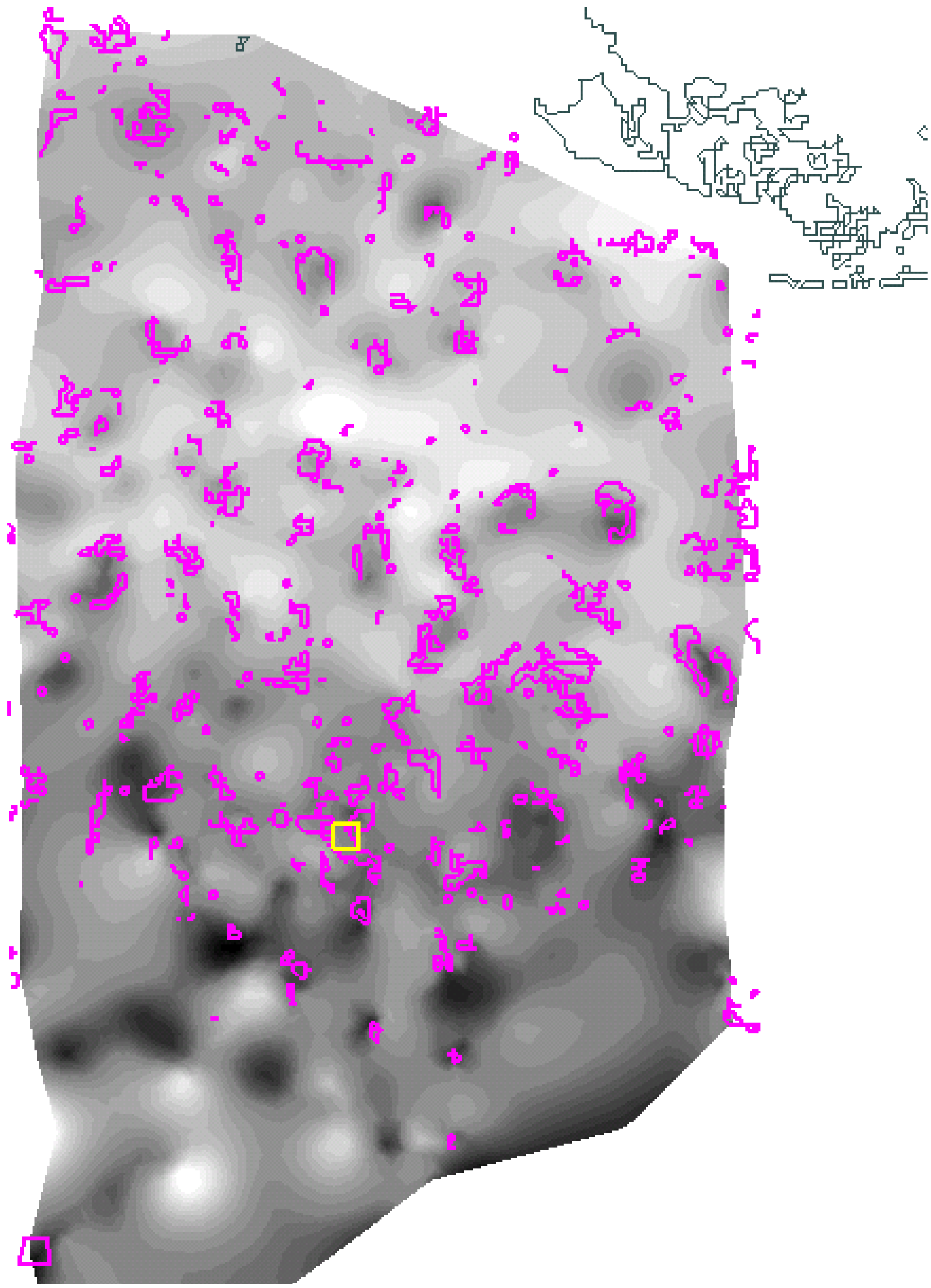

Figure 15. The outlines of discovered hydrocarbon reservoirs (cyan outlines) from Bascle et al. (2001) in many cases lie on or near topographic highs in the equivalent 12 ppg mudweight surface (dark gray shading indicates topographic highs).

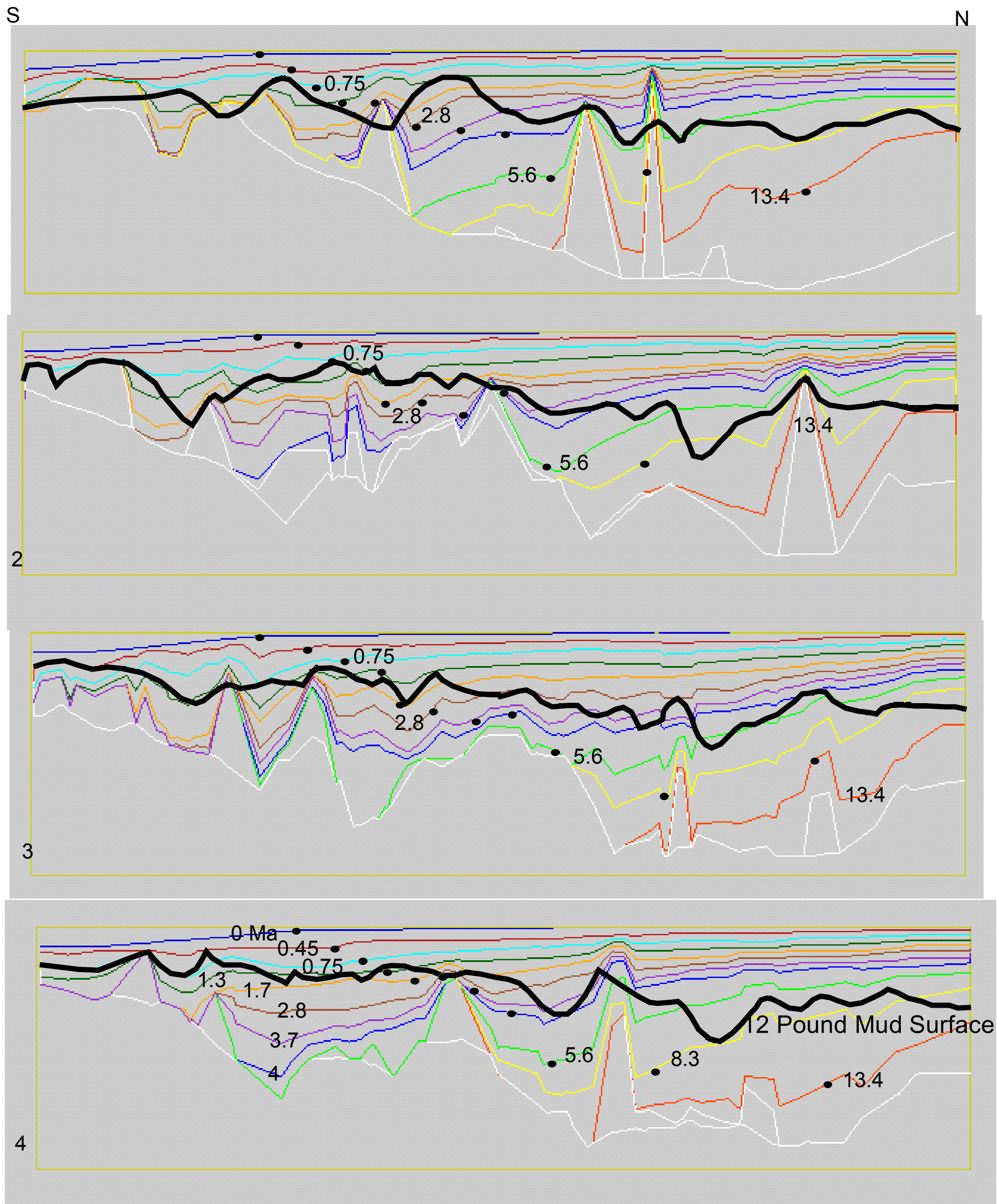

Figure 16. N-S sections through the GRI Louisiana Corridor showing the relationship of the 12 ppg equivalent mudweight surface (black line) to the time-stratigraphic horizons listed in Table 1 (colored lines). Section 3 runs through South Eugene Island Block 330. Sections 2 and 4 lie about a block to the west and east respectively. Section 1 lies about half way from SEI330 and the western border of the GRI Corridor. Black dots indicate the location of the paleo-shelf break according to Galloway et al. (1991) and Cornelius et al. (in press) at the time the time-stratigraphic horizons were deposited.

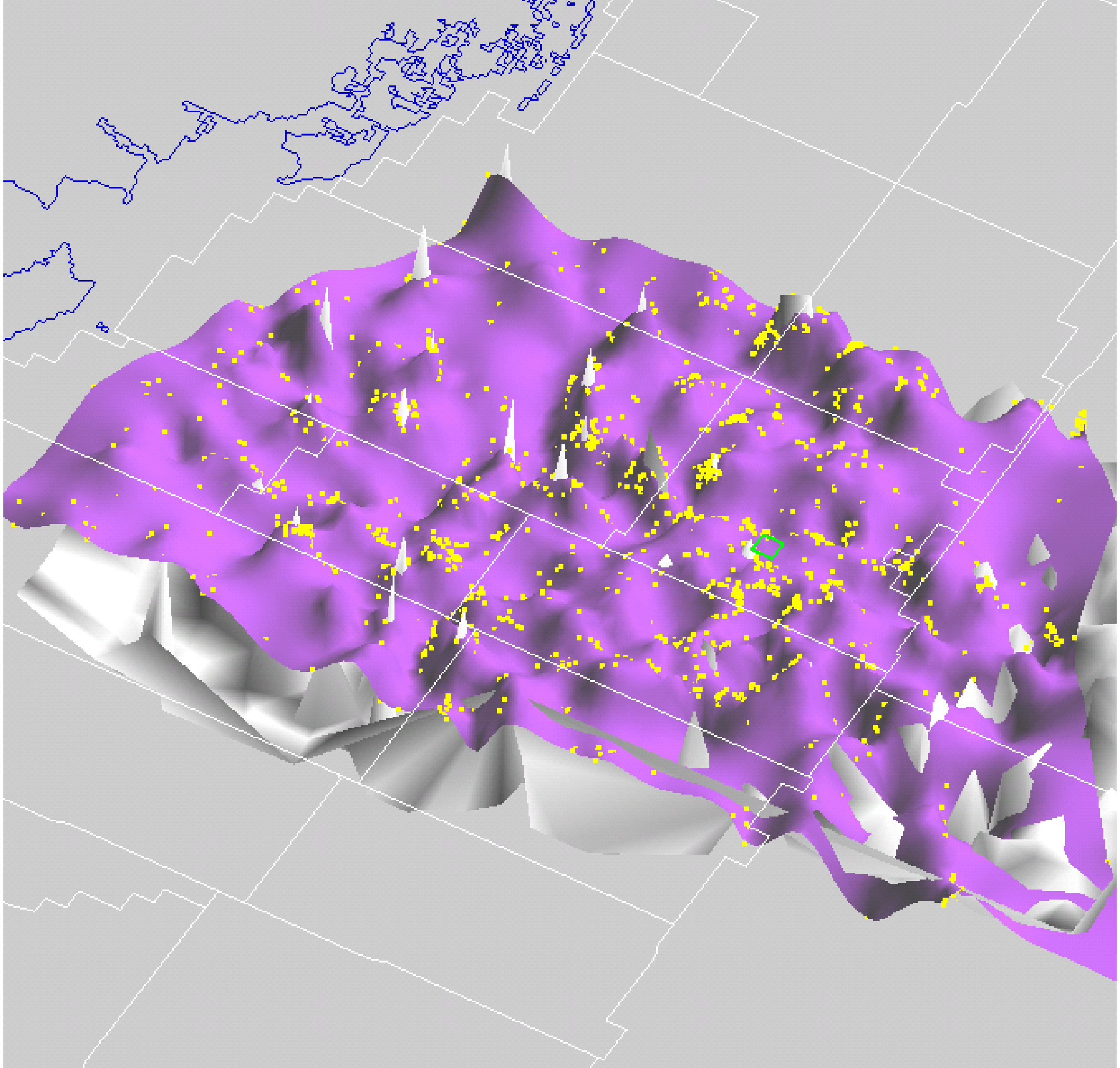

Figure 17. Top of salt surface (white), the krigged 12 ppg equivalent mudweight surface (top of overpressure or TOOP proxy, purple), and the computed depths of 12 ppg mudweights in individual wells (yellow dots). The TOOP tends to rise so as to stand topographically high near salt domes.

4. Chemical Data

a. Hydrocarbon Source Beds in Northern GoM

Hydrocarbon source rocks were deposited early in the Gulf of Mexico's rifting history (Jurassic-Lower Cretaceous) when seawater access was restricted and fluvial input was disorganized. Source beds of lesser importance in the GRI Corridor were also deposited during major Eocene marine transgressions. The most recent source rock compilation is by Gross et al. (1995), which we reproduce in Figure 18 below. Our compilation of published source rock analyses (Table 2) shows the importance of Eocene sources, but also shows the paucity of published pre-mid Cretaceous source rock analyses. This lack of data is not surprising, given the depth of these strata beneath much of the northern Gulf of Mexico.

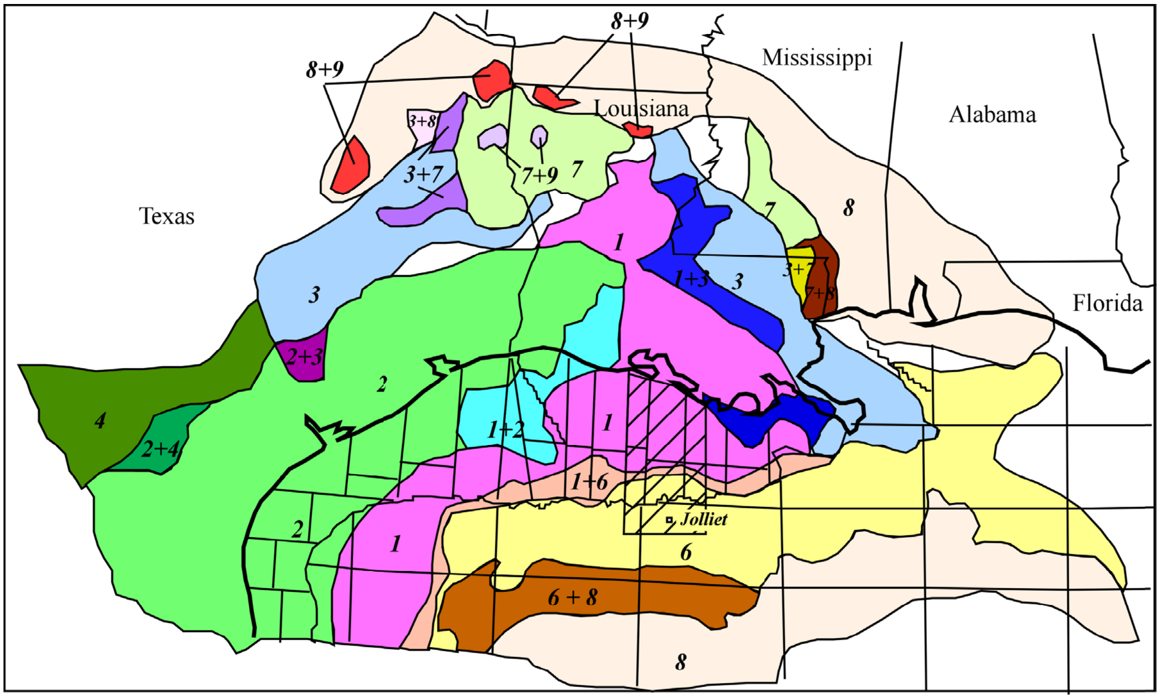

Map No	*Oil Age/Type*
1	*Tertiary/Marine+Intermediate*
2	*Tertiary Terrestrial*
3	*U. Cret (Turonian)/ Marine; Low Sulfur*
4	*U. Cret (Turonian) and L. Cret (Aptian)/Calcareous; Moderate Sulfur*
5	*L. Cret (Aptian)/Carbonate; elevated salinity (not on map)*
6	*U. Jurassic (Ththonian)/Marine; moderate to high sulfur*
7	*U. Jurassic (Tithonian)/Calcareous*
8	*U. Jurassic (Oxfordian (Smackover))/Carbonate; elevated salinity*
9	*Triassic (Eagle Mills)/Lacustrine*
◸	*GRI Corridor*

Figure 18. Hydrocarbon source rock map for the northern Gulf of Mexico Basin. Modified from Gross et al. (1995)

Table 2. Summary of hydrocarbon source rocks, northern Gulf of Mexico. References are in Appendix 3.

Age	(Ma)	Stratigraphic Units	Avg. TOC (samples)	Kerogen Type	Location	Study
NEOGENE						
U. Pliocene		Turbidites	0.44% (8)	III	Off Tx/La	Taylor/Arm
Miocene		Shale	0.71% (8)	III	Off. La.	Sassen/C
		Robulus "L" sands	0.57% (13)	III	Off La.	Pasley, et
PALEOGENE						
L-M Eocene	43-60	Cane R., Sparta & Wilcox	1 % (1045)	II/III	S. La.	McDade
M. Eocene	49.3-43	Cane River & Sparta Fms	3.3% (53)	II/III	S. La.	McDade
		Sparta Fm.	2.19% (150)	II	S-C. La.	Sassen
		Sparta Fm.	2.93% (45)	II	S La.	Sassen/C
L. Eocene	60-49.3	Wilcox Group	2.7% (49)	II/III	S. La.	McDade
U. Paleocene -L. Eocene		Wilcox Group	1.82% (80)	III	SW La.	Sassen
		Wilcox Group	0.44% (150)	III	N-C La.	Sassen
		Wilcox Group	1.46% (111)	III/II	S-C La.	Sassen
		Wilcox Group	0.88% (113)	III/II	SW La.	Sassen
		Wilcox Group	2.91% (25)	III/II	S. La.	Sassen/C
		Wilcox Group	1.62 (36)	III	La/Miss	Sassen et
L-U Paleocene		Midway Fm	0.81% (24)	III	SW La.	Sassen
		Midway Fm	2.32% (31)	III/II	SW Miss	Sassen
UPPER CRETACEOUS						
Campanain?		Austin Chalk	0.15% (24)	III	SW Miss	Sassen
Turonian-Santonian?		Eutaw Fm.	0.61% (12)	III	W-C Ms	Sassen
		Eutaw Fm.	0.97% (19)	III	SW Miss	Sassen
Cenomanian		Tuscaloosa Fm.	0.9% (??)	II/III	C. La.	Smith
		Tuscaloosa Fm.	1.53% (13)	II?	SW Ala	Mancini
		Tuscaloosa Fm.	0.62 (111)	III	S-C La.	Sassen
		Tuscaloosa Fm.	0.96% (19)	III/II	SW Miss	Sassen
		Tuscaloosa Fm	0.28% (36)	III	W-C Ms	Sassen
		Tuscaloosa Fm	0.62% (8)	??	S La.	Sassen/C
UPPER JURASSIC						
Kimmeridgian	144-142	Haynesville Fm	0.12% (17)	??	SW Ala	Mancini
Oxfordian		Smackover	0.25% (50?)	??	C La.+	Heydari
Oxfordian	150.5-144	Smackover-highstand	0.29%	??	SW Ala.	Mancini
		Smackover-transgressive & condensed section	0.81%	??	SW Ala	Mancini
Callovian	155.5-150.5	Norphlet	0.10%	??	SW Ala	Mancini
		DEEP-WATER GULF OF MEXICO				
TERTIARY						
L. Miocene & Lower Tertiary		??	2.0% (6)	II	Deep	Wagner
UPPER CRETACEOUS						
Maastrichtian-Santonian ?		Navarrro, Taylor, &Austin equiv.?	1.2% (19)		Deep	Wagner

A recent major maturity modeling study listed the important northern Gulf of Mexico source rocks as Eocene to Paleocene (centered about the Wilcox Formation), Upper Cretaceous (mostly centered about the Turonian Eagleford, Cenomanian Woodbine), Middle Cretaceous (Cenomanian and Tuscaloosa formations), Lower Cretaceous (Aptian to Valanginian), and Upper Jurassic(Tithonian and Oxfordian) (Colling, Alexander et al., 2001). The vertical separation between the Upper Cretaceous and Upper Jurassic horizons is not great in the GRI Corridor (see Figures 3 and 4). The upper Jurassic rocks are by far the most prolific sources in the northern Gulf of Mexico.

For the purpose of modeling, we follow Colling et. al. (2001) in grouping hydrocarbon source rocks in the Corridor into two stratigraphic intervals: Upper Jurassic and Eocene. Our Upper Jurassic source interval is 100 m thick and contains an average 5% TOC of Type II source with an HI~652 mg/g at the oil stage and 538 mg/g at the gas stage of maturation. This source interval underlies the entire northern Gulf as shown in Figures 3 and 4. It combines in one chronostratigraphic interval, bounded by the 131 and 127.7 Ma age horizons, the following sources estimated by E. Colling (p.c., 2002): Upper Cretaceous (2.5% TOC Type II over 30 m at 88-91 Ma with HI~450 mg/g), Lower Cretaceous (4% TOC Type II over 30 m at 120 Ma with HI~650), and Upper Jurassic (6% TOC Type II over 60 m at Ma with HI~700).

We also define a single Eocene source interval 30 m thick, bounded by 59 and 57.9 Ma time-stratigraphic horizons. This interval hosts Type III kerogen with an average TOC of 4% and HI~179 at the gas stage and 0.204 at the oil stage of maturation. This source rock extends about 100 km offshore and underlies the northern part of GRI Corridor only (Figures 3, 4; Table 2).

Table 3 summarizes our generalization of source rocks, and calculates the generation potential within the Corridor from the HI and TOC kerogen content. The generation potential is ~200 Bt (10^9 metric tonnes) or ~1430 x 10^9 Bbl (billion barrels – of oil and 173 Bt or ~ 8600 TSCF trillion standard cubic feet) of gas.

Table 3. The likely hydrocarbon source characteristics in the GRI Corridor are synthesized from Gross et al. (1995) and Colling et al. (2001). The Eocene source underlies only the northern half of the area. The generation potential is calculated according to the HI (redundant) shown. These HI are taken from standard (Braun and Burnham, 1990; Burnham and Braun, 1990) kinetic models for Type II kerogen and a simple kinetic model for the maturation of Type II/ III kerogen provided by John Hunt [p.c. 1991]. The kinetic models are discussed in the modeling report in this series. Data is from Bascle et al. (2001).

	Jurassic Type II Source		**Eocene Type II/III Source**	
Bed Thickness [m]	100		30	
Aerial Extent in Corridor [km^2]	125 x 201.8 = 25,230		125 x 93 = 11,630	
TOC [Wt %]	5		4	
	Oil Stage	Gas Stage	Oil Stage	Gas Stage
Initial Kerogen Mass [10^9 t]	313	313	34	34
HI Index [g HC/g TOC]	0.652	0.538	0.204	0.179
Generation Potential [10^9 t]	204 (195 oil)	168	6 (+ 2.4 CO_2)	6 (+ 2.4 CO_2)

b. Proven Hydrocarbon Resources in the GRI Corridor

Proven recoverable reserves (the sum of the cumulative production and the proved resources that remain to be produced) have been summed for the Corridor study area from the data of Bascle et al. (2001) (Table 4). Unproved recoverable resources are small compared to the proven total (~14% in the northern part of the GRI Corridor and <2% in the south), so the proven recoverable resource provides a reasonably accurate measure of the volumes of recoverable hydrocarbons that initially lay at currently drillable depths. The total in-place hydrocarbons in these reservoirs is 2 to 3 times greater as recoveries are ~30 to 50%. As shown in Table 4, there are about 11.1 x 10^9 barrels of oil (1.37 billion tonnes) of commercially reservoired hydrocarbons in the Corridor. On a mass basis there is about twice as much reservoired gas as oil. The known hydrocarbon resources in the GRI Corridor represent less than 0.8% of the hydrocarbons generated (Table 3), indicating the petroleum system in the Corridor, and in the northern Gulf of Mexico as a whole, is very leaky. We further define this "leakiness" in Volume V of this series of reports.

Table 4. Hydrocarbon resources in the GRI Corridor that have been proven to be recoverable (= recovered to date plus proven reserves = R_c). Data are from Bascle et al. (2001).

	Reservoired Hydrocarbons (Imperial Units)	**Reservoired Hydrocarbons (Metric Units)**
Oil	2.62 x 10^9 bbl	0.46 × 10^9 t
Gas	45 TCF	0.91 × 10^9 t
Gas-oil ratio	17,175 scf/bbl	1.98 (kg gas/kg oil)
Total	11.1 × 10^9 bboe	1.37 × 10^9 t (=R_c)

c. The Gas-Oil Ratio (GOR)

The gas-oil ratio reflects both phase separation of gas and oil from supercritical gas-oil, and the mixing and interaction of late-generated gas with earlier-generated gas and oil. Figure 19 shows initial potential and production test gas-oil ratios in the GRI Corridor. The figure was prepared by extracting data from header logs. The data suggest gas and oil have fractionated from supercritical gas-oil at depths below ~15,000 ft in the corridor. The data also suggest that late-generated gas has been added to both phases because they are shifted to higher GOR from Thompson's "equilibrium" lines.

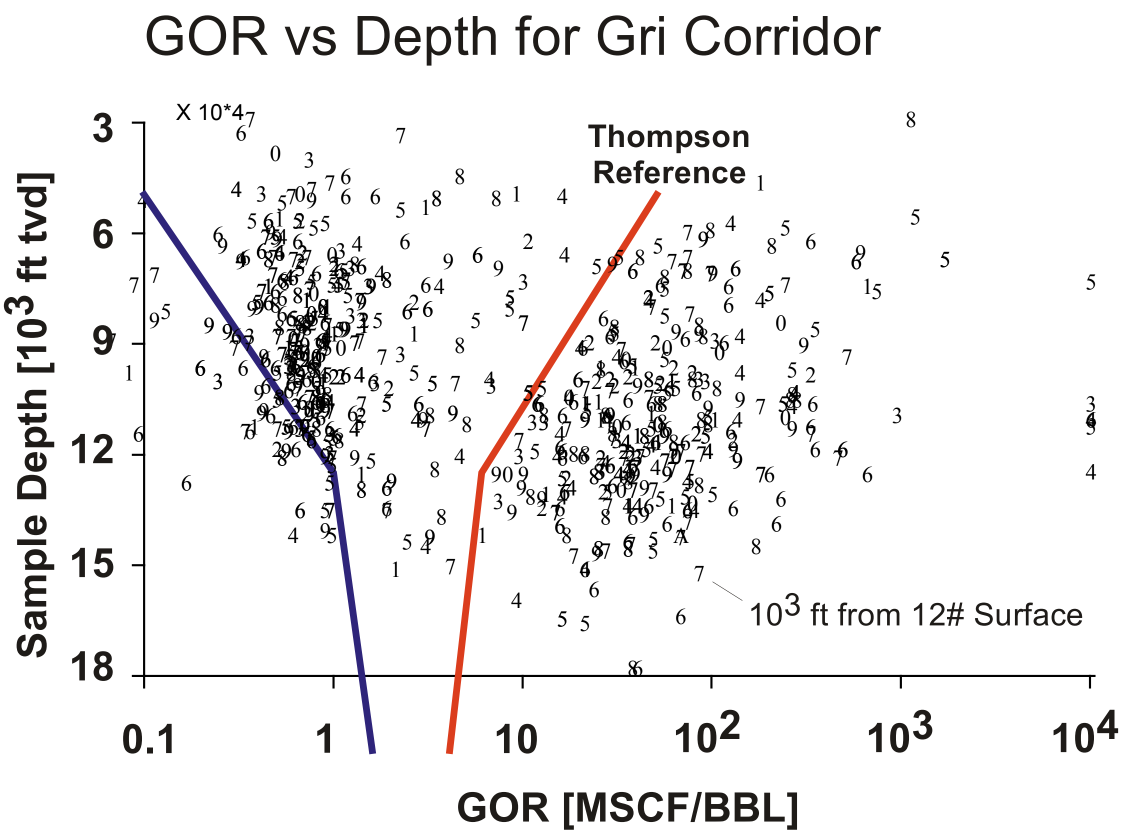

Figure 19. Gas-oil ratio of hydrocarbons recovered in 1287 initial production and production well tests. Header log data reporting the production rates of gas in thousands of cubic feet per day is divided by the header log production rate of oil or condensate in barrels per day to obtain the GOR in thousands of cubic feet per barrel. The production test data are plotted according to the true vertical depth of the collection point and the calculated GOR using an alphanumeric symbol. The symbol indicates the distance between the location of the point at which the hydrocarbon sample was collected and the 12 pound mud surface. For example 7 indicates the collection point was 7,000 feet above or below the 12 pound mud surface, an "A" indicates 10,000 ft separation, etc. The data show no apparent relationship to the 12 pound equivalent mud surface. The red and blue curves show GOR vs. depth for paired residual-oil and exsolved vapor (condensate) for North Sea hydrocarbons carefully selected for lack of alteration (p.c. Keith Thompson, 1998). Oils, and gases that exsolve from them, would be expected to lie on these two trends if there is no excess (free) gas in the system. The production test oils fall to the right (gas-rich side) of Thompson's residual oil trend, and the condensates have much higher gas-liquid ratios than those in phase equilibria with residual oils, indicating that free gas has been added.

The MMS data compiled in our GoCAD database shows that gas dissolved in Corridor oil increases in a quasi-regular way with reservoir pressure. This suggests that the oils in the Corridor are generally saturated with gas.

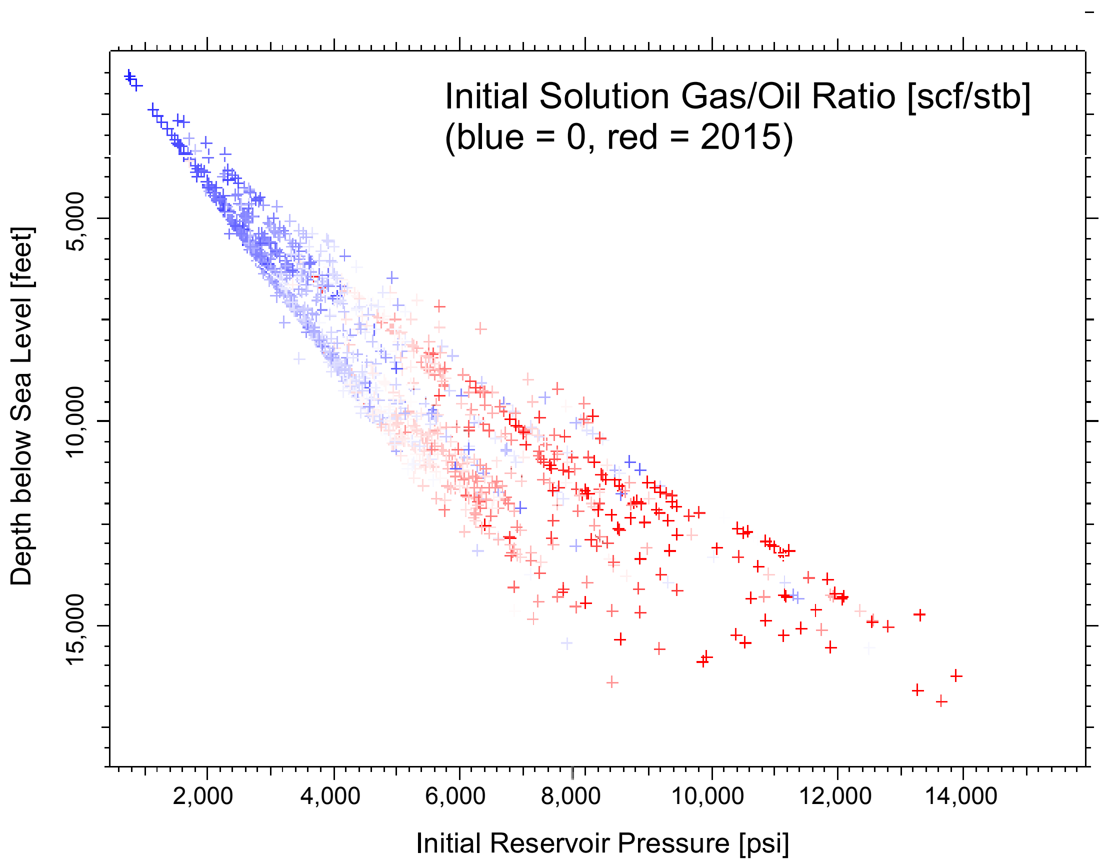

Figure 20. Initial solution gas-oil ratio is shown in color (r to b represents 0 to 2015 scf/stb). The symbols are plotted according to the initial reservoir pressure and reservoir depth of the sampled oil. Data are from the MMS Atlas (Bascle et al., 2001).

D. Results and Discussion

The work reported here was funded under a proposal to test 10 corollaries of a new capillary seal hypothesis. The first two hypotheses can be addressed by data compiled this report. They are:

- Hypothesis I: The position of a seal is predictable (safety implications) from physical chemistry principles and stratigraphic information.
- Hypothesis II: The expulsion of fluids (water and hydrocarbon) from overpressured zones below the top seal will be focused to topographic highs of the top of overpressure seal.

The capillary seal hypothesis holds that the basin interiors are divided into pressure compartments largely by capillary seals. Capillary seals form when two immiscible phases (a non-wetting hydrocarbon phase and brine) are present in the pore space of a grain-size layered media. Laboratory experiments demonstrate that these seals form easily and have exceedingly low permeability (Shosa and Cathles, 2001).

The capillary seal hypothesis has a host of potentially important implications that are fully discussed by Cathles (2001). One is that, since the strongest capillary contrast is between gas and water, the toughest seal (e.g., the seal most resistant to leakage) will form where hydrocarbon phase separation occurs. This seal is an attractive candidate to form the top of overpressure (TOOP). If so, the depth of the TOOP can be predicted from the depth (pressure) at which hydrocarbon phase separation occurs, and the locations of appropriately grain-size layered sediments. The "toughest" seal forms at the top of the complex of overpressured compartments. The interior compartments are divided by weaker seals. The top seal is like the rind of an orange.

The second hypothesis is that the tough gas-charged top seal (orange rind) will preferentially leak where it is topographically highest. At these locations it is buried by less sediment and hence, for a common degree of overpressuring, most vulnerable to hydrofracture. If topographic highs in the top of overpressure do leak preferentially, they should draw hydrocarbon and aqueous fluids from surrounding areas, and traps near these leak points should be preferentially filled with hydrocarbons.

The data we have compiled in this report address these two hypotheses, and also document lateral changes in basin temperature gradient that are large enough to affect maturation models.

The top of overpressure (TOOP) configuration documented in this report does <u>not</u> support a phase change control for the top of overpressure. The equivalent 12 ppg mudweight surface is too spiky to track a hydrocarbon phase boundary if the separated liquid and vapor phases have a relatively constant composition. The spikes in the TOOP cut across such large changes in fluid pressure that tracking the phase boundary in even a compositionally variable oil would be difficult. This difficulty is strengthened by the probability that the leaking hydrocarbons have become increasingly gas-rich with time due to progressive source maturation. Increased gas depresses the phase boundary, requiring phase separation to occur at greater, not shallower, depths. Thus, over time, the

TOOP at vent sites should become progressively deeper than at non-vent sites if its depth were controlled strictly by phase. The topography at the top of overpressure reflects controls other than phase behavior.

There is strong evidence for the late introduction of gas in many areas. For example, the gas at Eugene Island Block 330 is more mature (R_e=1.5 %) than the oil (R_e=0.8%) (Whelan et. al., 1994). Oils in the Corridor have been massively washed by gas (see third report in this series by Losh and Cathles). Figure 19 suggests that gas has been added to both the gas-rich and oil-rich products of phase separation.

As discussed in Cathles (2001) the leak zones appear to be persistent. They are generally localized in faults and shear zones bounding salt diapirs and salt sheets at the margins of salt-withdrawal minibasins. These leak points are topographic highs in the TOOP (the faults themselves are not highs, but they may bound pressure compartments that are highs), but the overpressure highs are not controlled by hydrocarbon chemistry (rather, they appear to be controlled by faulting at salt margins). The depth of the TOOP might have been controlled by the chemistry of the hydrocarbons initially, but continued hydrocarbon venting has since changed the relationship of gas-oil ratio TOOP depth to the opposite of that predicted. Capillary seals may be involved. Gas may reduce the permeability around the spiky vents by forming capillary blockages, but faulting controls the location of the vents. The orange model must be changed to a spiked orange model, where the spikes have rupture-prone central cores that have persistently leaked (Cathles, 2001).

From the above discussion it is clear that the second hypothesis is supported by the GoCAD data. As shown in Figure 15, topographic highs (spikes) in the TOOP are surrounded by hydrocarbon reservoirs. Topographic highs in the TOOP thus appear to have been persistent hydrocarbon vents. This may be because permeability is maintained in the active faults that host the vents. It may be because leaking gas has created a fringe of capillary blockage that protects and localizes the vents. In any event, topographic highs in the TOOP are clearly a favorable exploration indicator.

Finally the GoCAD analysis of temperature gradients in the Corridor indicates relatively sharp and significant lateral changes on the scale of 50 km on the shelf. Sharp lateral changes in near-surface temperature gradient are also observed in shallow sediment data in the deepwater Gulf of Mexico by Colling et. al. (2001). These workers identified domains of differing geothermal gradient separated by transform fault-like discontinuities. Their data consist mostly of heat flow measurements in the upper few meters of the sediment column. Our data suggest that the anomalous thermal gradients persist to >5 km depth.

The temperature gradient variations documented by Colling et. al. (2001) appear to be related to basement fabric. The causes of the temperature gradient variations we document are not clear. The spatial resolution of the data we have access to is not sufficient to address whether they are related, as seems likely, to the combined effects of salt thermal conductivity and rapid minibasin sedimentation. However, the variations in temperature gradient are clearly important. At 5 kilometers depth, temperature along a 19°C/km thermal gradient diverges from that along a 25°C/km gradient by 30°C. 102º versus 132°C assuming a seafloor temperature of 7°C). This difference is as large as that separating the oil and gas stages of maturation.

E. Recommendations

Because of its apparent importance in controlling hydrocarbon migration, the causes of the persistent leakage that appears to be occurring through spikes in the top of overpressure need further investigation. Methods of investigation might include modeling of fluid venting to determine the factors that could sufficiently focus flow, documentation of inorganic alteration around the sites and inversion of this data to indicate cumulative leakage, and targeted seismic analysis, especially 4 component analysis that could simultaneously define the structure of the leak zones and the presence of gas and establish the relationship between spikes in the top of overpressure surface and active sea floor hydrocarbon seeps.

The causes of the abrupt changes in temperature gradient in Figure 10b should be investigated. Proving the reality of the anomalies, and determining their cause sufficiently to predict the occurrence of similar anomalies at past times when important hydrocarbon source beds were maturing are clearly important goals if models of hydrocarbon maturation are to accurately guide exploration on a local (~50 km) scale.

Acknowledgements

We gratefully acknowledge Landmark Graphics Corporation for their software grant to Cornell University under their University Affiliates Program. This software was used in preparing the seismic interpretations for the Tiger Shoals and Jolliet Fields.

Appendix 1: Data in the GRI Corridor GOCAD Project

Data Included in Gri_Final.prj

GOCAD, a comprehensive modeling and visualization program vended by T-surf (http://www.t-surf.com/), was used to create geologic models of the study sites for the Louisiana Corridor Project. The final GoCAD data compilation, *GRI_Final.prj*, is included on the project CD-ROM. The data include:

- GRI Corridor geology (horizons, faults, top and bottom of salt)
    - regional
    - local
        - Tiger Shoal
        - South Marsh Island 9
        - South Eugene Island 330 area
        - Jolliet area
- WHOI hydrocarbon chemical analyses
- Geochemical indices derived from the WHOI analyses
- Geochemical indices at Tiger Shoals from Texaco analyses
- Gas chemistry and isotopic measurements
- 12 pound equivalent mud surface
- Data extracted from MMS CD-ROM (Bascle et al., 2001)

Sources of Data in Gri_final.prj

Data comes from four sources:

- *Geological maps:* The surfaces that describe the strata and faults in the GoCAD project were generated from a variety of oil-company maps as described in the test of this report. Scanned structure-stratigraphic maps (Regional SEI-330 and SMI-9) and Landmark (Tiger Shoals and Jolliet) horizon surfaces were input into GoCAD. Several stratigraphic intervals (including salt), and faults (except the regional and SMI-9 areas) are also represented as surfaces.
- *Well Log Header Data:* Mud weight and initial and production test data were extracted from well log headers as described in the body of this report.
- *Chemical Analyses:* Analyses of hydrocarbon samples mostly collected and analyzed by us for this project but including also other analysis data.
- *Cultural and Production data from the **Atlas of Gulf of Mexico Gas and Oil Sands** (Gulf Atlas) CD-ROM produced in 2001 by the U.S. Department of the interior Mineral Management Service (MMS):* Cultural data such as shorelines, block boundaries, sand reservoir outlines, production data, gas-oil ratio, and a host of other data were extracted from this source and placed in the GoCAD Project.

Data Structure of *Gri_final.prj*

GoCAD organizes data in *Point Sets, Curves,* and *Surfaces*. These visual elements can be individually turned on and off by checking or unchecking them on a list. In the GRI GoCAD Project:

- Strata and faults are input as GoCAD *surfaces*,
- Cultural reference data (block boundaries, shoreline, reservoir sand outlines, etc.) are input as *curves*, and
- Chemical, pressure, block hydrocarbon resources, etc. are input as property vectors of *point data*.

Surface data:

The surfaces are named using the following convention *Area_age_name*:

- The first part of the name is the study *area* (e.g., Jolliet, SEI, etc.)
- Next is the *age* of the strata (if determined)
- The last element is the *name* of the surface
- Note that a few surfaces (e.g., Jolliet salt) are grouped surfaces and are found in the Group hierarchy in the GoCAD model.

Line Data:

Cultural data was mostly extracted from the MMS database described below. Line data in the *Gri_final.prj* file includes:

- *3D_Outline:* The outline of the GRI Corridor
- *AllFields_NoData:* The outline of all hydrocarbon fields
- *Boundaries_Atlas:* Outline of lease block areas in northern Gulf
- *Reg_blockgrid:* Block outlines in the GRI Corridor
- *SEI_block_330:* Outline of South Eugene Island Block 330
- *ShoreAtlasUTM:* Outline of shoreline

Point Data:

Geochemical data consists of 4 point sets, each with several properties that can be displayed in color-coded scale.

- *All_GRI_oils* contains concentration or chromatogram peak area data for 229 hydrocarbon compounds from WHOI high resolution gas chromatography/mass spectrometry analyses.
- *All_geoch_indicies* contains selected indices derived from the WHOI analyses, related to gas washing, biodegradation, oil source and maturity.
- *Gases* contains analyses of gas composition and isotopic ratios.
- *TigerShoals_Indicies* contains somewhat different indices produced in a Texaco project.

Toop_12mud_data are points where wells intersect the equivalent 12 pound mud surface.
Excess Fluid P is the initial reservoir pressures of the MMS Atlas with hydrostatic pressure subtracted.
SEI330_temperatures is temperature and other point data in SEI 330 area

MMS Atlas Data is temperature, pressure, API, GOR, etc., at the center point of each sand.

Each point can have many associated properties. For example all the properties of each sample point in *All_GRI_oils* is the relative abundance of 111 hydrocarbon compounds, there are 22 different indices associated with each of the sample locations in *All_geoch_indicies,* etc. Tables A1-1 to A1-3 define the properties of the point sets listed above with multiple properties.

Extraction of MMS Atlas Data:

The ***Atlas of Gulf of Mexico Gas and Oil Sands*** (Gulf Atlas) CD-ROM was produced in 2001 by the U.S. Department of the interior Mineral Management Service (MMS) and includes data compiled from federal and state fields as of January 1, 1999. This Atlas groups hydrocarbon accumulations into plays with common geological and production characteristics. The plays are subdivided into fields, pools, sands, and reservoirs.

The data in the atlas are organized in a geographic information system (GIS) which links map graphics and tables of data together in a digital environment. Digital data in the Atlas includes: (1) attribute data of sand body reservoirs, reservoir pools, fields, and plays, and (2) GIS files of the boundaries of fields and plays. The GIS files can be viewed in ArcView, a spatial data-viewer program from Environmental Systems Research Institute, Inc. (ESRI). We wrote macros to extract this data and format it in a form that allowed its incorporation in the GoCAD project *Gri_Final.prj*. The data was compiled for the GoCAD model in the following manner. One or more reservoir sand with associated tabulated data is located within each field. A single GoCAD location point was generated for each reservoir by calculating an average (center) position of the reservoir outline from the GIS data (shapefile). The tabulated attributes are associated with this point in the GoCAD project.

Bibliography

2001, The Atlas of Northern Gulf of Mexico Gas and Oil Sands, eds., Bascle, B., Nixon, L.D., and Ross, K.M., U.S. Department of the Interior, Mineral Management Service.

Table A1-1. Point sets, curves, and surfaces in GoCAD project *GriFinal.prj*.

Point Sets	
All_GRI_oils	Chromatographic peak heights or absolute concentrations for 111 oils in GRI Corridor
All_geoch_indices	Biomarker and gas washing indices derived from oil analyses; includes additional data from SEI330 and Tiger Shoals area
GASES	Compositional and Isotopic analyses of gases in Corridor
GOM_Atlas_data	Data from MMS GoM Atlas
Excess Fluid P	Excess pressure in GRI Corridor (pore pressure-hydrostatic pressure) from MMS Atlas
SEI330_temperatures	Temperature data in SEI330 area
Toop_12mud_data	12 pound mud equivalent pore pressure in 2131 Corridor wells

Curves	
3D_outline_0	GRI Corridor outline
AllFields_NoData	Outline of all hydrocarbon fields in northern GoM
AllStateFields_NoData	Outline of all state hydrocarbon fields in northern GoM
Boundaries_Atlas	Outline of Edition Boundaries in northern GoM
Reg_blockgrid	Outlines of block boundaries in GRI Corridor
SEI_Block _330	Outline of South Eugene Island Block 330
ShoreAtlasUTM	Coastline of northern GoM

Surfaces	
Jol	Jolliet, Green Canyon Block 184 4 time-stratigraphic surfaces as described in Table 1 of text All major faults Top of salt is under groups heading
Reg	GRI Corridor 11 time-stratigraphic horizons as described in Table 1 of text Top and bottom of salt
SEI	South Eugene Island Block 330 Area 7 time-stratigraphic horizons as described in Table 1 of text LF and OI sands under groups heading 6 major faults Top and bottom of salt Sea surface
SMI	South Marsh Island Block 9 6 time-stratigraphic surfaces of unknown age (see Table 1 of text) One of these surfaces (Cp_9_sand) is under group heading
TS	Tiger Shoals 4 time-stratigraphic surfaces as described in Table 1 of text Faults
Toop	Top of overpressure as proxied by 12 ppg equivalent mudweight surface TOOP surface is krigged version of the 12 ppg point set

Table A1-2. Geochemical biomarker and other indices in indicated point sets in *GriFinal.prj*.

All_geoch_indices	
29DbR/29DbR+bbR	C29-13b(H), 17a(H) 20R/(C29-13b(H), 17a(H) 20R-diasterane+C29-13b(H), 17b(H) 20R-sterane) Source
29S/R	29aaS/29aaR Source and maturity
API_gravity	
BT+DBT+MDBT	Sum of benzothiophene, dibenzothiophene, and methyldibenzothiophene (sulfur). Source
Biodeg_ratio	(nC8-nC41)/(i-C10+i-C11+i-C13+i-C14+i-C15+i-C16+i-C18+i-C19+i-C20)
Break_no	Carbon number of lightest n-alkane that is not fractionated from liquid oil. See Report 3.
C27/(27+28+29)reg_ster	5a(H),14a(H),17a(H),20(R)-Cholestane/(5a(H),14a(H),17a(H),20(R)-Cholestane + 24 – methyl-5a(H),14a(H),17a(H),20(R)- Cholestane + 24-ethyl 5a(H),14a(H),17a(H),20(R)-Cholestane). Source
Carb_pref	((nC23+25+27+29+31)/(24+26+28+30+32)) +((nC25+27+29+31+33)/(24+26+28+30+32)). Maturity
DBT/P	(sum dibenzothiophenes/sum phenanthrenes). Source
H35R/H31-35R_index	35abR/(31abR+32abR+33abR+34abR+35abR). Source and biodegradation
MNR	2-MN/1-MN . Maturity and source
Oleanane_index	30O/30ab hopane . Source/age (angiosperms).
Ph/nC18	phytane/n-C18. Biodegradation index for oils of similar source and maturity
Pr/Ph	pristane/phytane. Source
Pr/nC17	pristane/n-C17. Biodegradation index for oils of similar source and maturity
Re%_MPI1	0.6*(1.5*(2-MP + 3-MP)/(P + 1-MP + 9-MP)) + 0.4 Maturity
SampleNumber	
TA/TA+MA	R28TA/(R28TA+aRC29MA) Maturity
TA20,21/TA26,27,28	20TA+21TA/(S26TA+R26TA&S27TA+S28TA+R27TA+R28TA) Maturity
Tricyclic/17aH_index	C24H44 Tricyclic Terpane/17a(H),21b(H)-Hopane Source and Maturity
n-alk_mass_depl	Mass nC10+ deficiency relative to unfractionated oil. See Report 3
n-alk_slope	Δ(ln mole fraction of n-alkane)/ Δ n-alkane carbon number See report 3
Sum_nC25-nC41	Self-explanatory. Affected by biodegradation; also tracks maturity, phase separation

Table A1-3. GoM Atlas reservoir point set properties in GoCAD project *GriFinal.prj*.

GoM_Atlas_Data	
API	Oil API gravity (API units)
BGI	Initial gas formation volume factor (scf/cf)
BOI	Initial oil formation volume factor (bbl/stb)
CUMBOE	Cumulative BOE produced (bbl)
CUMGAS	Cumulative gas produced (Mcf)
CUMOIL	Cumulative oil produced (bbl)
DISCBOE	Discovered BOE (bbl) [P_RECBOE + U_RECBOE]
DISCGAS	Discovered gas (Mcf) [P_RECGAS + U_RECGAS]
DISCOIL	Discovered oil (bbl) [P_RECOIL + U_RECOIL]
GAREA	Gas total area (acres)
GOR	Gas-oil ratio (Mcf/bbl)
GTHK	Gas average net thickness (ft)
GVOL	Gas total volume (acre-ft)
OAREA	Oil total area (acres)
OTHK	Oil average net thickness (ft)
OVOL	Oil total volume (acre-ft)
P_RECBOE	Proved recoverable BOE (bbl)
P_RECGAS	Proved recoverable gas (Mcf)
P_RECOIL	Proved recoverable oil (bbl)
P_REMBOE	Proved remaining recoverable BOE (bbl)
P_REMGAS	Proved remaining recoverable gas (Mcf)
P_REMOIL	Proved remaining recoverable oil (bbl)
PERMEABILI	Average permeability (millidarcy)
PI	Initial pressure (psi)
PLAY_NUM	Play number
POROSITY	Average porosity (decimal)
PROP	Proportion oil (decimal)
RSI	Initial solution gas-oil ratio (scf/stb)
SDPG	Sand pressure gradient (psi per foot)
SDTG	Sand temperature gradient (degrees F per 100 ft)
SPGR	Gas specific gravity (decimal at 60 degrees F and 15.025 psia)
SW	Water saturation (decimal)
TAREA	Total area (acres)
THK	Total average net thickness (ft)
TI	Initial temperature (degrees F)
TVOL	Total volume (acre-ft)
U_RECBOE	Unproved recoverable BOE (bbl)
U_RECGAS	Unproved recoverable gas (Mcf)
U_RECOIL	Unproved recoverable oil (bbl)
WDEP	Water depth (ft)
YIELD	Yield (stb/MMcf) – gas reservoir's recoverable condensate divided by recoverable gas

Table A1-4. Gases point set properties in GoCAD project GriFinal.prj.

Gases	
%C1	Mole percent methane
%C2	Mole percent ethane
%C3	Mole percent propane
%nC4	Mole percent n-butane
%iC4	Mole percent iso-butane
%nC5	Mole percent n-pentane
%isoC5	Mole percent iso-pentane
%C6+	Mole percent C6+
%CO2	Mole percent CO_2
%N2	Mole percent N_2
Gas_dryness	Mole percent C1/(Mole percent C1-C6+)
Del 13C CO2	$\delta^{13}C$ CO_2 PDB
Del 13C C1	$\delta^{13}C$ methane
Del 13C C2	$\delta^{13}C$ ethane
Del 13C C3	$\delta^{13}C$ propane
Del 13C iC4	$\delta^{13}C$ isobutane
Del 13C nC4	$\delta^{13}C$ n-butane
Del 13C C5	$\delta^{13}C$ n-pentane
Del D C1	δD methane

Appendix 2: Loading and Use of the GRI GoCAD Project

Display of the GoCAD Geological and Geochemical database.

1) Start GoCAD
2) When the initial window comes up, click on "File" (as shown) and select "Open Project"

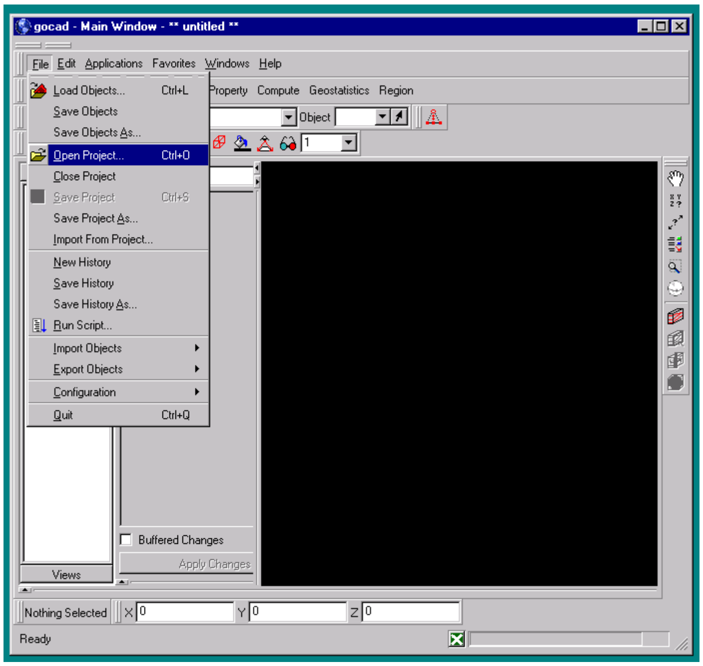

3) Select the Project titled *GRI_Final.prj*. If you are using the CD-ROM, this project will be the only one that appears in the pop-up window. Click "OK."

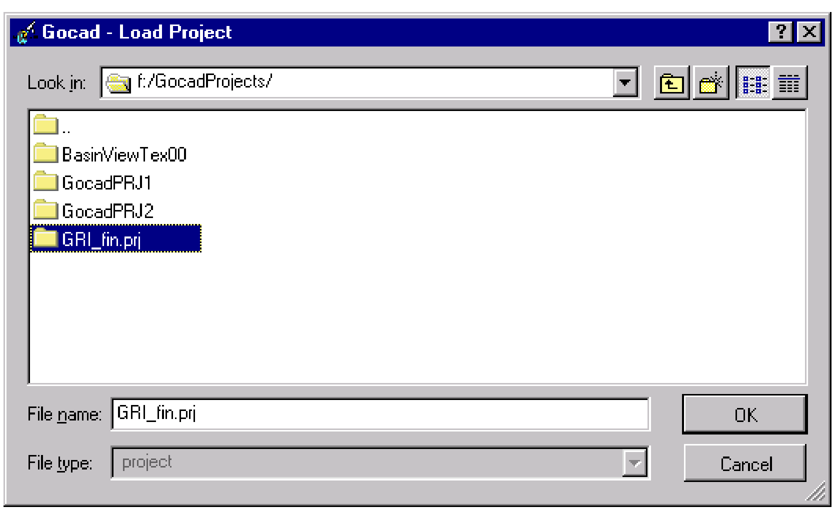

4) When the project has loaded, the display window will still be black. Click on Objects in the left-hand workspace in the GoCAD window, as shown below. Several types of Objects appear in the window to its right. Click on "Point Set" to display geochemical, temperature, and pressure data points. Click on "Curve" to display map features that consist of lines or curves. Select the items you want to display, as shown. Here, the point set "All_geoch_indices" and the curve "3D_outline" are shown. At first, GoCAD will display an arbitrary item within the selected point set. Here, break number is shown.

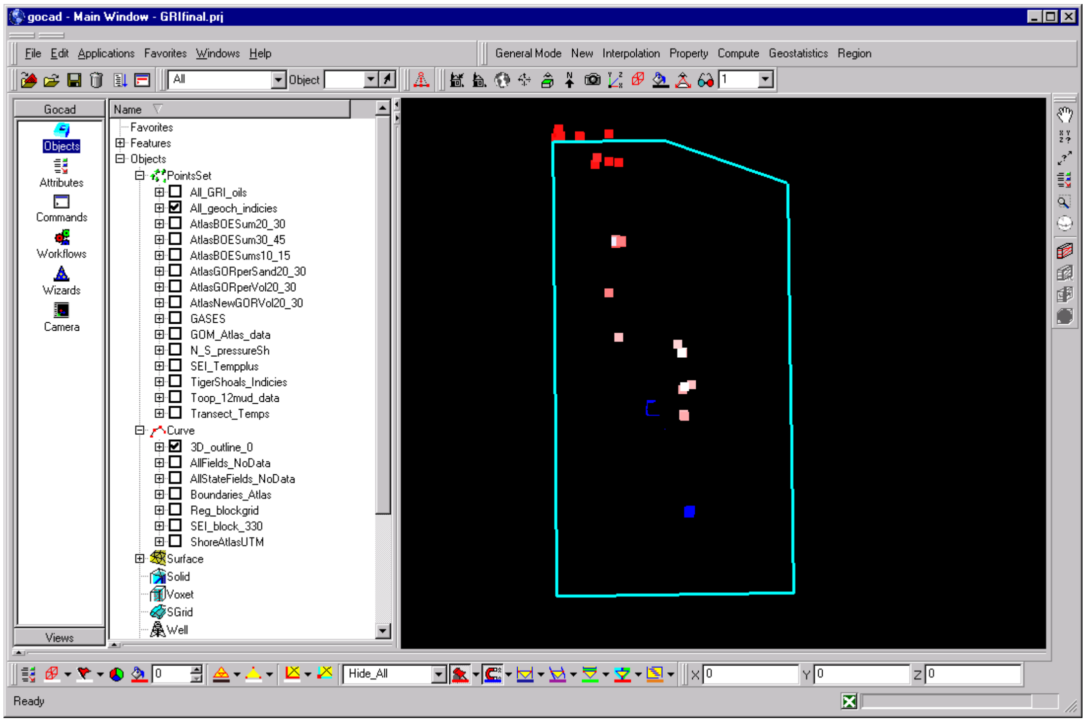

5) To select the desired data in the point set, click on "Property" in the left-hand workspace. Then, click on the first arrow button immediately to the right of the "Object" text box (this appears just above the pull-down menu in the example below). Select the same point set on the pull down menu that was selected in step (4)

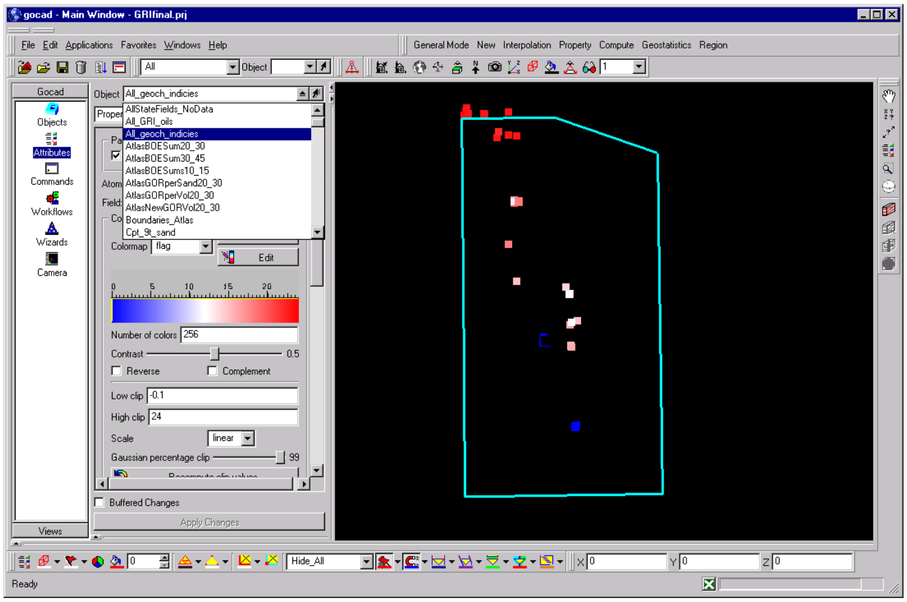

6) To select a particular index within the "All_geoch_indices" point set, click on "Atomic Property", as shown below, and select the desired index in the pull-down window. Here, 29S/R is selected. Be sure that the name of the point set you want is shown in the "Object" text window (from Step 5). If it is not, pull down the menu using the arrow button immediately next to the text window and select the desired point set. If you change the point set in the "Object" text window, be sure to also go back to step (4) and select that point set in the "PointSet" list. At the same time, de-select any undesired point sets. Follow this same procedure for any point set.

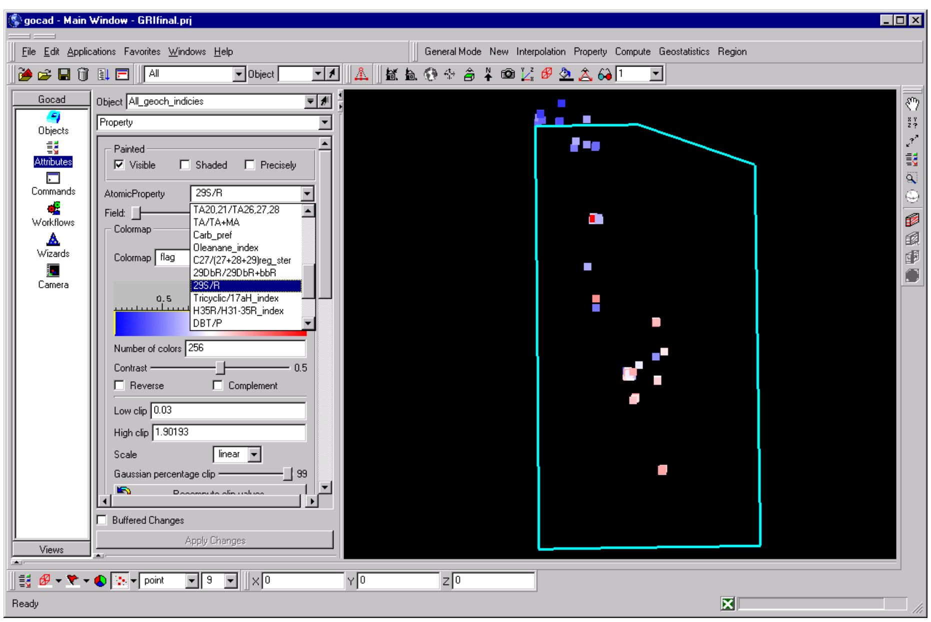

7) To select surfaces, such as stratigraphic horizons, faults, and top of overpressure, return to the left-hand workspace in the GoCAD window. Click on "Objects" and then on "Surfaces". Select the desired surfaces from the list, as shown below.

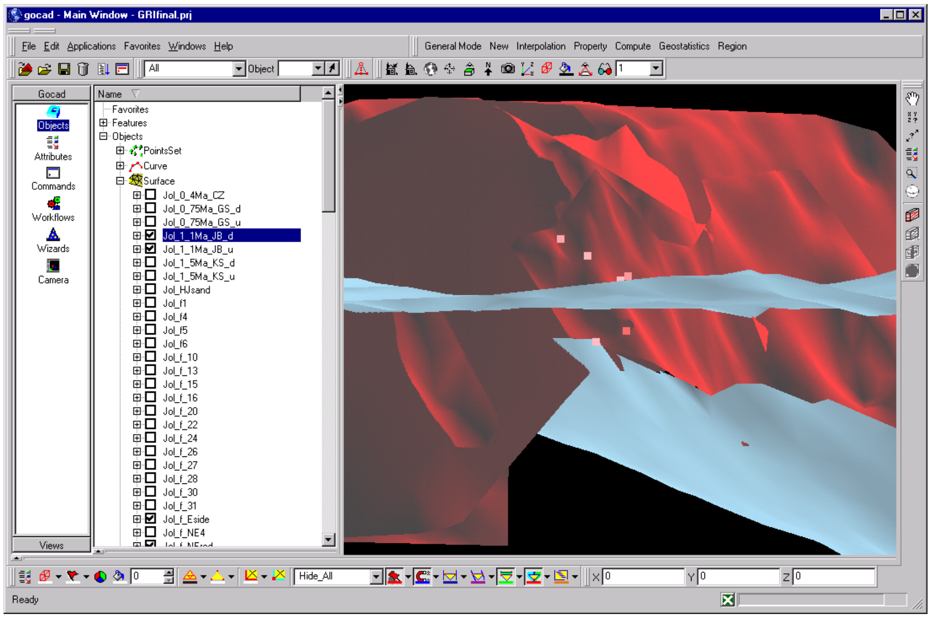

In this display window, several operations have been performed. After selecting the desired surfaces (here, 1.1Ma sands and several faults at the Jolliet Field), the area of interest was enlarged by zooming in and repositioning the field of view. To do this, first make sure the proper cursor mode is operational by clicking on the small hand in the toolbar on the right side of the GoCAD display window. Zooming is done by holding down the right mouse button and simultaneously dragging the mouse. Repositioning the field of view is performed by holding down the middle mouse button (or, for a two-button mouse, holding down the left and right buttons at the same time) and dragging the mouse in the desired direction. Finally, the view was rotated to allow better viewing of the relationship between the datapoints and the geology. Rotation is accomplished by holding down the left mouse button and dragging the mouse in the desired direction.

To restore the view to an easily recognized reference frame, click on the small globe in the toolbar just above the display window, then on the icon that shows an eyeball looking down on a block. These actions cause GoCAD to display the entire point set with north at the top of the display window.

Appendix 3: References for Hydrocarbon Sources in the Northern Gulf of Mexico

Bissada, K.K., Katz, B.J., Barnicle, S.C., and Schunk, D.J., 1990, On the origin of the hydrocarbons in the Gulf of Mexico basin-a reappraisal: *in* D. Schumacher and B.F. Perkins (eds.), Geochemistry of Gulf Coast oils and gases: *Gulf Coast Section SEPM Foundation Ninth Annual Research Conference Proceedings*, p. 163-171.

Dow, W.G., 1984, Oil Source beds and oil prospect definition in the upper Tertiary of the Gulf Coast: *Gulf Coast Association of Geological Societies Transactions,* v. 34, p. 329-339.

Echols, J.B., Zimmerman, R.K., and Goddard, D.A., 1994, An integrated geochemical and geological approach for determining Hydrocarbon generation-migration patterns: Central Gulf Coast Basin: *Gulf Coast Association of Geological Societies Transactions*, v. 44, p. 193-203.

Kennicutt, M.C., McDonald, T.J., Comet, P.A., Denoux, G.J., and Brooks, J.M., 1992, The origins of petroleum in the northern Gulf of Mexico: *Geochimica et Cosmochimica Acta*, v. 56, p.1259-1280.

McDade, E.C., Sassen, R., Wenger, L., and Cole, G.A., 1993, Identification of organic-rich lower Tertiary shales as petroleum source rocks, south Louisiana: *Gulf Coast Association of Geological Societies Transactions*, v. 43, p. 257-267.

Sassen, R., 1990, Lower Tertiary and Upper Cretaceous source rocks in Louisiana and Mississippi: implications to Gulf of Mexico crude oil: *American Association of Petroleum Geologists Bulletin*, v. 74, p. 857-878.

Taylor, G.D., and Armentrout, J.M., 1990, Rock geochemistry and relationships to produced oils from Upper Pliocene turbidites, High Island area, Gulf of Mexico: *in* D. Schumacher and B.F. Perkins (eds.), *Geochemistry of Gulf Coast oils and gases: Gulf Coast Section SEPM Foundation Ninth Annual Research Conference Proceedings*, p. 151-161.

Wagner, B.E., Sofer, Z. and Claxton, B.L., 1994, Source rock in the lower Teriary and Cretaceous, deep-water Gulf of Mexico: *Gulf Coast Association of Geological Societies Transactions*, v. 44, p. 729-736.

Wenger, L.M., Sassen, R., and Schumacher, D., 1990, Molecular characteristics of Smackover, Tuscaloosa, and Wilcox reservoired oils in the eastern Gulf Coast: in D. Schumacher and B.F. Perkins (eds.), Geochemistry of Gulf Coast oils and gases: *Gulf Coast Section SEPM Foundation Ninth Annual Research Conference Proceedings*, p. 37-57.

Bibliography

Alexander, L. and J. Handschy, 1998, Fluid flow in a faulted reservoir system, South Eugene Island Block 330 Field, offshore Louisiana: *AAPG Bulletin*, v. 82, p. 387-411.

Alexander, L. L. and P. B. Flemings, 1995, Geologic evolution of a Pliocene-Pleistocene salt withdrawal mini-basin: Eugene Island Block 330, offshore Louisiana: *AAPG Bulletin*, v. 82, p. 387-411.

Bascle, B., L. D. Nixon, et al., 2001, Atlas of Gulf of Mexico Gas and Oil Sands, U. S. Department of Interior, Minerals Management Service.

Blackwell, D. D. and J. L. Steele, 1992, Geothermal map of North America, Boulder, Geological Society of America Inc.

Braun, R. L. and A. K. Burnham, 1990, Mathematical model of oil generation, degradation, and expulsion: *Energy and Fuels*, v. 4, p. 132-146.

Burnham, A. K. and R. L. Braun, 1990, Development of a detailed model of petroleum formation, destruction, and expulsion from lacustrine and marine source rocks: *Organic Geochemistry*, v. 16(1-3), p. 27-39.

Cathles, L. M., 2001, Capillary seals as a cause of pressure compartmentation in sedimentary basins: *Petroleum Systems of Deep-Water Basins: Global and Gulf of Mexico Experience*, Houston, Texas, GCSSEPM, p. 561-571.

Colling, E. L., R. J. Alexander, et al., 2001, Regional mapping and maturity modeling for the northern deep water Gulf of Mexico: *GSCSEPM Transactions*.

Colling, E. L., R. J. Alexander, et al., 2001, Regional Mapping and Maturity Modeling for the Northern Deep Water Gulf of Mexico: *Petroleum Systems of Deep-Water Basins: Global and Gulf of Mexico Experience*, Houston, Texas, GCSSEPM, p. 87-111.

Cook, D. and P. D'Onfro, 1991, Jolliet field thrust structure and stratigraphy, Green Canyon Block 184, offshore Louisiana: *Trans. Gulf Coast Assoc. Geol. Socs.*, v. 41, p. 100-121.

Diegel, F., J. Karlo, et al., 1995, Cenozoic structural evolution and tectonostratigraphic framework of the northern Gulf Coast continental margin: in M. P. A. Jackson, D. G. Roberts and S. Snelson, ed., Salt tectonics: a global perspective: Tulsa, Amer. Assoc. Petrol. Geol., v. Memoir 65**,** p. 109-152.

Erendi, A. and L. M. Cathles, 2001, Gas capillary inhibition to oil production: *Petroleum Systems of Deep-Water Basins: Global and Gulf of Mexico Experience*, Houston, Texas, GCSSEPM, p. 607-618.

Feng, J., R. T. Buffler, et al., 1994, Laramide orogenic influence on late Mesozoic-Cenozoic subsidence history, western deep Gulf of Mexico Basin: *Geology*, v. 22, p. 359-362.

Galloway, W., D. Bebout, et al., 1991, Cenozoic: in A. Salvador, ed., The Gulf of Mexico Basin: Bolder, The Geological Society of America, v. J**,** p. 245-324.

Galloway, W., P. Ganey-Curry, et al., 2000, Cenozoic depositional history of the Gulf of Mexico Basin: *AAPG Bulletin,* v. 84, p. 1743-1774.

Holland, D. S., J. B. Leedy, et al., 1990, Eugene Island Block 330 field-U.S.A., offshore Louisiana: in E. A. Beaumont and N. H. Foster, ed., Structural traps III, tectonic fold and fault traps: AAPG Treatise of Petroleum Geology Atlas of Oil and Gas Fields: Tulsa, American Association of Petroleum Geologists, v., p. 103-143.

MacDonald, I. R., N. L. Guinasso, et al., 1994, Gas hydrate that breaches the sea floor on the continental slope of the Gulf of Mexico: *Geology*, v. 22, p. 699-702.

McBride, B., 1998, The evolution of allochthonous salt along a megaregional profile across the northern Gulf of Mexico Basin: *AAPG Bulletin*, v. 82, p. 1037-1054.

McFarlan, E. and L. S. Menes, 1991, Lower Cretaceous: in A. Salvador, ed., The Gulf of Mexico Basin: Boulder, The Geological Society of America, v. J, p. 181-204.

Meulbroek, P., 1997, Hydrocarbon phase fractionation in sedimentary basins: Geological Sciences Ph.D. Thesis, Ithaca, Cornell, p. 345.

Meulbroek, P., 1998, Phase fractionation at South Eugene Island Block 330: *Organic Geochemistry*, v. 29, p. 223-229.

Nagihara, S., J. G. Sclater, et al., 1996, Heat flow in the western abyssal plain of the Gulf of Mexico: Implications for thermal evolution of old oceanic lithosphere: *Journal of Geophysical Research*, v. 101(B2), p. 2895-2913.

Peel, F., G. Cole, et al., 2001, Paleographic evolution of the deep-water frontier of the Gulf of Mexico during the Later Jurassic to Cretaceous: a radical reappraisal and its impact on the petroleum system: *AAPG Annual Meeting Abstracts,* v., p. A155-A156.

Revil, A. and L. M. Cathles, 2001, The porosity-depth pattern defined by 40 wells in Eugene Island South Addition, Block 330 Area, and its relation to pore pressure, fluid leakage, and seal migration: *Petroleum Systems of Deep-Water Basins: Global and Gulf of Mexico Experience*, Houston, Texas, GCSSEPM, p. 687-712.

Salvador, A., 1991, Triassic-Jurassic: in A. Salvador, ed., The Gulf of Mexico Basin: Bolder, The Geological Society of America, v. J, p. 131-180.

Sassen, R. and I. R. MacDonald, 1994, Evidence of structure H hydrate, Gulf of Mexico continental slope: *Organic Geochemistry*, v. 22(6), p. 1029-1032.

Shosa, J. D. and L. M. Cathles, 2001, Experimental investigation of capillary blockage of two phase flow in layered porous media: *Petroleum Systems of Deep-Water Basins: Global and Gulf of Mexico Experience*, Houston, Texas, GCSSEPM, p. 721-740.

Smith, D. L. and W. T. Dees, 1982, Heat flow in the gulf coastal plain: *Journal of Geophysical Research*, v. 87(B9), p. 7687-7693.

Temple, R. F., D. L. Harrington, et al., 1977, Monthly temperature and salinity measurements of continental shelf waters of the northwestern Gulf of Mexico, 1963-1965, Washington, NOAA, p. 26.

Winker, C. D., 1982, Cenozoic shelf margins, northwestern Gulf of Mexico: *Gulf Coast Assoc. Geol. Soc. Trans.*, v. 32, p. 427-448.

Winker, C. D., 1984, Clastic shelf margins of the post-Comanchean Gulf of Mexico, implications for deepwater sedimentation: *GCSSEPM*, v. 5th Bob F. Perkins Research Conference, p. 109-117.

Woods, R., A. Salvador, et al., 1991, Pre-Triassic: in A. Salvador, ed., The Gulf of Mexico Basin: Denver, Geol. Soc. Amer., Decade of North American Geology, p. 109-130.